The Second Subunit of DNA Polymerase Delta Is Required for Genomic Stability and Epigenetic Regulation[1][OPEN]

Jixiang Zhang, Shaojun Xie, Jinkui Cheng, Jinsheng Lai, Jian-Kang Zhu, and Zhizhong Gong*

State Key Laboratory of Plant Physiology and Biochemistry, College of Biological Sciences, China Agricultural University, Beijing 100193, China (J.Z., J.C., Z.G.); Shanghai Center for Plant Stress Biology, Shanghai Institutes for Biological Sciences, Chinese Academy of Sciences, Shanghai 200032, China (S.X., J.-K.Z.); Department of Horticulture and Landscape Architecture, Purdue University, West Lafayette, Indiana 47906 (S.X., J.-K.Z.); and State Key Laboratory of Agrobiotechnology, China National Maize Improvement Center, Department of Plant Genetics and Breeding, China Agricultural University, Beijing 100193, China (J.L.)

ORCID IDs: 0000-0002-1641-8650 (J.Z.); 0000-0002-6719-9814 (S.X.); 0000-0001-5134-731X (J.-K.Z.).

DNA polymerase δ plays crucial roles in DNA repair and replication as well as maintaining genomic stability. However, the function of *POLD2*, the second small subunit of DNA polymerase δ, has not been characterized yet in Arabidopsis (*Arabidopsis thaliana*). During a genetic screen for release of transcriptional gene silencing, we identified a mutation in POLD2. Whole-genome bisulfite sequencing indicated that POLD2 is not involved in the regulation of DNA methylation. *POLD2* genetically interacts with *Ataxia Telangiectasia-mutated and Rad3-related* and *DNA polymerase α*. The *pold2-1* mutant exhibits genomic instability with a high frequency of homologous recombination. It also exhibits hypersensitivity to DNA-damaging reagents and short telomere length. Whole-genome chromatin immunoprecipitation sequencing and RNA sequencing analyses suggest that *pold2-1* changes H3K27me3 and H3K4me3 modifications, and these changes are correlated with the gene expression levels. Our study suggests that POLD2 is required for maintaining genome integrity and properly establishing the epigenetic markers during DNA replication to modulate gene expression.

DNA replication is a fundamental process that duplicates both genetic information (DNA sequence) and epigenetic information (DNA methylation and histone modifications). During DNA replication in each cell cycle, nucleosomes are reassembled onto newly synthesized DNA to maintain the chromatin structures (Probst et al., 2009). Three key DNA polymerases are essential for DNA replication: DNA polymerase (Pol) α, Pol δ, and Pol ε. It is a well-accepted concept that, after a short RNA-DNA primer extension by the Pol α-primase complex, Pol ε and Pol δ replace Pol α and perform the bulk of DNA synthesis in the leading and lagging strand, respectively (Burgers, 2009).

Pol δ is a highly accurate DNA polymerase that is essential for DNA replication, repair, and recombination and thus for genome integrity (Prindle and Loeb, 2012). Dysfunction of Pol δ results in genomic instability and cancer (Church et al., 2013; Palles et al., 2013). Pol δ in mammals consists of four subunits: the catalytic subunit p125 (POLD1, corresponding to Pol3p in yeast (*Saccharomyces cerevisiae*) and CDC6 in *Saccharomyces pombe*); the accessory subunit p50 (POLD2, corresponding to Pol31p in *S. cerevisiae* and CDC1 in *S. pombe*); p68 (POLD3, corresponding to Pol32p in *S. cerevisiae* and CDC27 in *S. pombe*); and the smallest subunit p12 (POLD4, corresponding to CDM1 in *S. pombe*; Prindle and Loeb, 2012). The Pol31p and Pol32p subunits in yeast also interact with DNA polymerase zeta (Pol ζ) to participate in DNA translesion synthesis and mutagenesis (Johnson et al., 2012). Recent studies suggest that Pol δ may replicate both strands (Johnson et al., 2015; Miyabe et al., 2015).

Several DNA-replication factors have been reported to help mediate transcriptional gene silencing (TGS) in plants (Liu and Gong, 2011). In Arabidopsis (*Arabidopsis thaliana*), mutations in replication factor C1 (RFC1), Pol ε, Pol α, and replication protein A2A (RPA2A) can suppress gene silencing in a DNA methylation-independent manner (Elmayan et al., 2005; Kapoor et al., 2005; Xia et al., 2006; Liu et al., 2010a, 2010b). These mutants are hypersensitive to DNA damage and exhibit reduced

[1] This work was supported by the Natural Science Foundation of China (grants 31330041 and 31121002). J.Z. was supported by Chinese Universities Scientific Fund Number 2013YJ002.

* Address correspondence to gongzz@cau.edu.cn.

The author responsible for distribution of materials integral to the findings presented in this article in accordance with the policy described in the Instructions for Authors (www.plantphysiol.org) is: Zhizhong Gong (gongzz@cau.edu.cn).

J.Z. and Z.G. conceived the original research plans; J.Z. performed most of the experiments; S.X., J.C., and J.L. provided bioinformatic analysis; J.Z. and Z.G. designed the project and wrote the article with contributions of all the authors; J.-K.Z. discussed the data and complemented the writing.

[OPEN] Articles can be viewed without a subscription.

www.plantphysiol.org/cgi/doi/10.1104/pp.15.01976

telomere length and increased genomic instability. BRUSHY1 (BRU1), TEBICHI, and FASCIATA1 (FAS1, chromatin assembly factor 1) are also related to DNA damage and TGS (Takeda et al., 2004; Ramirez-Parra and Gutierrez, 2007; Inagaki et al., 2009). Because all of these proteins are involved in the DNA replication and repair pathway, we refer to this pathway as the DNA replication and repair-mediated TGS pathway (DRR-TGS pathway). However, the molecular mechanism of this pathway is not well known.

Repressor of silencing 1 (ROS1), a 5-meC DNA glycosylase/demethylase, and its homologous proteins DEMETER and DEMETER-like 2-3, are essential for maintaining the expression of endogenous genes and transgenes through active DNA demethylation (Gong et al., 2002; Zhu, 2009). In a previous study, we performed a genetic screen for additional *ROS* genes by using a transgenic Arabidopsis line that carries a T-DNA insertion expressing both the *ProRD29A:LUC* (*firefly luciferase* reporter driven by the stress-responsive *RD29A* promoter) gene and the *Pro35S:NPTII* (*neomycin phosphotransferase II* driven by the CaMV *35S* promoter) gene. Using this screen, we identified several genes in the RNA-directed DNA methylation (RdDM) pathway whose mutations silence *Pro35S:NPTII* because of the reduced expression of *ROS1*, indicating that the RdDM pathway positively modulates *ROS1* expression (Huettel et al., 2006; Li et al., 2012). One of these mutants isolated from the screen was *defective in meristem silencing 3* (*dms3-4*; Li et al., 2012). DMS3 is a silencing factor in RdDM that coordinates the formation of the DDR complex by defective in RNA-directed DNA methylation 1 and RNA-directed DNA methylation 1 and that facilitates Pol V transcript (Law and Jacobsen, 2010).

In this study, we used the *dms3-4* mutant to identify genes whose mutations release the silencing of *Pro35S:NPTII*, and we cloned *POLD2* from a *pold2-1* mutant. Whole-genome bisulfite sequencing (BS-seq) indicated that *pold2-1* does not change DNA methylation. Combining chromatin immunoprecipitation (ChIP)-seq with RNA-seq data, we found a high correlation between H3K27me3 and H3K4me3 modification and gene expression caused by the *pold2-1*. We also found that *pold2-1* exhibits sensitivity to DNA-damaging reagents, short telomere length, and genomic instability, including a high frequency of homologous recombination (HR). These results suggest that POLD2 is a new component in DRR-TGS pathway, which does not affect the DNA methylation and H3K9me2, but H3K27me3 and H3K4me3 modification. The altered H3K27me3 and H3K4me3 correlate with the changes of the expression of specific genes caused by *POLD2* mutation.

RESULTS

Isolation of a New Component in the DRR-TGS Pathway

dms3-4 was identified during a genetic screen for mutants that silence *Pro35S:NPTII* in a transgenic Arabidopsis line carrying expressed *ProRD29A:LUC* and *Pro35S:NPTII* (C24 accession, which was used as the wild type in this study; Li et al., 2012). We performed a forward genetic screen using an ethyl methanesulfonate (EMS)-mutagenized *dms3-4* population to isolate the mutants that release the silenced *Pro35S:NPTII* in *dms3-4*. We isolated several mutants, including *pold2-1*, *rfc1-4*, *ubiquitin-specific protease26* (*ubp26-5*), and *histone deacetylase 6* (*hda6-11*) in this screen (Fig. 1A; Supplemental Fig. S1). The *dms3-4* mutant was kanamycin sensitive because of the silencing of *Pro35S:NPTII* caused by the reduced expression of *ROS1*, while *pold2-1*, *rfc1-4*, and *ubp26-5* partially rescued the expression of *NPTII* in the *dms3-4* background (Fig. 1B) and *hda6-11* fully recovered the expression of *NPTII*. UBP26 is a H2B deubiquitination enzyme that is identified in a genetic screening for releasing silencing of *ProRD29A:LUC* and *Pro35S:NPTII* in *ros1-1* (Sridhar et al., 2007). HDA6 is a histone deacetylase that is involved in mediating DNA methylation and TGS (Murfett et al., 2001; Aufsatz et al., 2002; Probst et al., 2004). However, the expression level of *ROS1* was not greatly restored in these mutants (Fig. 1C). *TSIs* are endogenous TGS loci (Steimer et al., 2000), the expression of which is altered in some mutants involved in DNA methylation, histone modification, or DNA replication (Steimer et al., 2000; Xia et al., 2006; Yin et al., 2009; Liu et al., 2010a, 2010b). The expression of *TSIs* was increased in these isolated mutants (Fig. 1D). Interestingly, although *pold2-1* suppresses the silenced *Pro35S:NPTII* in the *dms3-4* mutant, the expression of *NPTII* in the *pold2-1* single mutant was lower than in the wild type (Fig. 1B). To confirm the role of *POLD2* in controlling the TGS of *Pro35S:NPTII*, we crossed *pold2-1* with other TGS-related mutants. ROS1 and ROS4 (IDM1) are DNA demethylation factors, and *ros1* and *ros4* exhibited kanamycin sensitivity due to the silencing of *Pro35S:NPTII* (Li et al., 2012). The double mutants *pold2-1 ros1-1* and *pold2-1 ros4-1* were resistant to kanamycin (Fig. 1E). *pold2-1* also suppressed the kanamycin-sensitive phenotype in *nrpd1-8* and *nrpe1-14* (Fig. 1E). However, *pold2-1* had little effect on the *ProRD29A:LUC* locus in *dms3-4*. Like mutants of DNA replication-related proteins (Elmayan et al., 2005; Xia et al., 2006; Yin et al., 2009; Liu et al., 2010a, 2010b), *pold2-1* failed to suppress the silenced *ProRD29A:LUC* in the *ros1-1* mutant (Fig. 1F). These results indicate that *pold2-1* suppresses the TGS of *Pro35S:NPTII* and that POLD2 is a newly identified component in the DRR-TGS pathway.

Map-Based Cloning of *POLD2*

The F1 progeny of *pold2-1 dms3-4* backcrossed with *dms3-4* had a kanamycin-sensitive phenotype like that of *dms3-4* (Fig. 2A), and the F2 progeny showed a kanamycin-sensitive to kanamycin-resistant ratio of about 3:1 (177:56; Fig. 2B), indicating that the *pold2-1* allele is recessive and caused by a single nuclear gene mutation. *pold2-1* mutant plants were much smaller and flowered earlier than the wild type (Supplemental Fig. S2B). To clone *POLD2*, we crossed *pold2-1 dms3-4* (C24) with the *dms3-1* mutant (Columbia-0 [Col-0]). The mutants

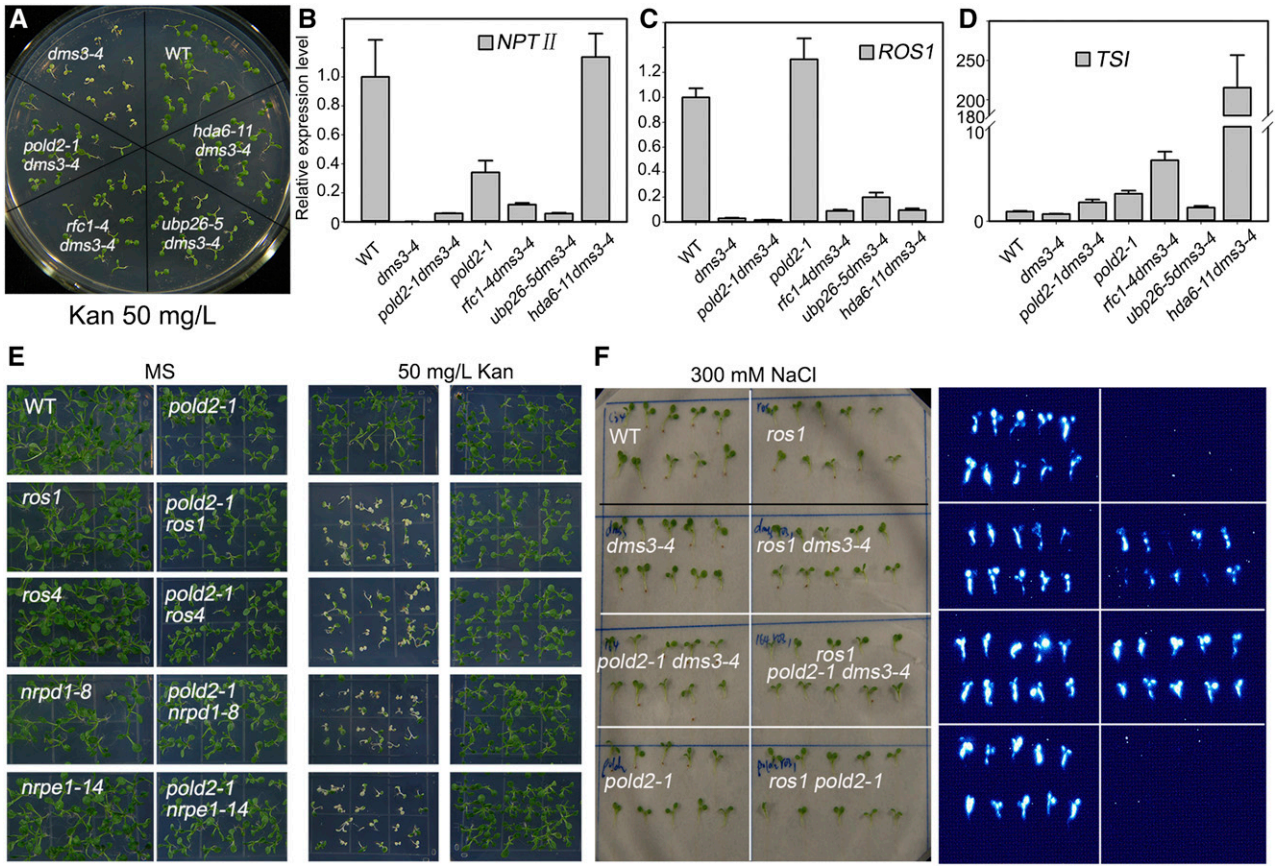

Figure 1. Isolation of mutants that suppress the kanamycin sensitivity of the *dms3-4* mutant. A, The phenotype of the wild type (WT), *dms3-4*, and suppressors of *dms3-4* growing on MS medium supplemented with 50 mg/L kanamycin. B, Relative expression of *NPTII* in the wild type, *dms3-4*, and suppressors of *dms3-4*. C, Relative expression of *ROS1* in the wild type, *dms3-4*, and suppressors of *dms3-4*. D, Relative expression of *TSI* in wild type, *dms3-4*, and suppressors of *dms3-4*. For B, C, and D, RNAs were extracted from 7-d-old seedlings. Values were normalized to the expression level of the references gene (*UBI*). Two independent experiments (each with three technical replicates) were done with similar results. Values are means ± SE, $n = 3$, from one experiment. E, *pold2-1* released the silencing of *35S:NPTII* in *ros1*, *ros4*, *nrpd1*, and *nrpe1*. The growth phenotype of the wild type, *pold2-1*, *ros1*, *ros4*, *nrpd1-8*, *nrpe1-14*, and double mutants *pold2-1 ros1*, *pold2-1 ros4*, *pold2-1 nrpd1-8*, and *pold2-1 nrpe1-14* on MS containing 0 or 50 mg/L kanamycin (Kan). F, *pold2-1* could not restore the expression of silenced *RD29A:LUC* caused by the *ros1* mutant. Luminescence imaging of the *RD29A:LUC* transgene. The indicated plants were treated with 300 mM NaCl for 3 h followed by luminescence imaging.

with a kanamycin-resistant phenotype were isolated from the F2 progeny. The mutated position in *pold2-1* was mapped at the end of chromosome 2, between BAC clones T28M21 and F18O19. A G-A mutation located at 1,170 nucleotides from the putative start codon was identified in *AT2G42120* (Fig. 2C). Because the mutated nucleotide is located at a splicing site between the fifth intron and the sixth exon, we sequenced the various transcripts using OligodT reverse-transcribed cDNAs. Unlike *POLD2* in the wild type, the misspliced allele in *pold2-1* produced several forms of transcripts (a total of five transcripts were identified from 23 clones). Among them, four transcripts produced premature stop codons, and one transcript missing 6 bp caused deletion of two amino acids and mutation of one amino acid, which might result in the translation of a protein with reduced function (Fig. 2D). To confirm that the kanamycin-resistant and retarded-growth phenotype was caused by the *POLD2* mutation, we complemented the *pold2-1 dms3-4* double mutant with the full-length *POLD2* genomic sequence. The transgenic progeny showed kanamycin sensitivity on Murashige and Skoog (MS) plates containing 50 mg/L kanamycin and grew normally in the absence of kanamycin (Fig. 2E). The other two constructs, *Pro35S:FLAG-HA-POLD2* and *ProPOLD2:POLD2-GFP*, could also complement the *pold2-1* phenotypes (Fig. 2E). The T-DNA insertion mutant *pold2-2* (762B02) was embryo lethal (Supplemental Fig. S2A), indicating that *POLD2* is an essential gene in Arabidopsis. We crossed *pold2-1* with *pold2-2-/+*, and about one-half of the F1 progeny showed more severe dwarf phenotypes than the *pold2-1* mutant, indicating that *pold2-1* protein dosage influences the plant growth phenotype (Supplemental Fig. S2B). To determine whether the transcript missing 6 bp in *pold2-1* is functional in plants, we transferred this transcript driven by the *35S* promoter (*Pro35S:pold2-1*)

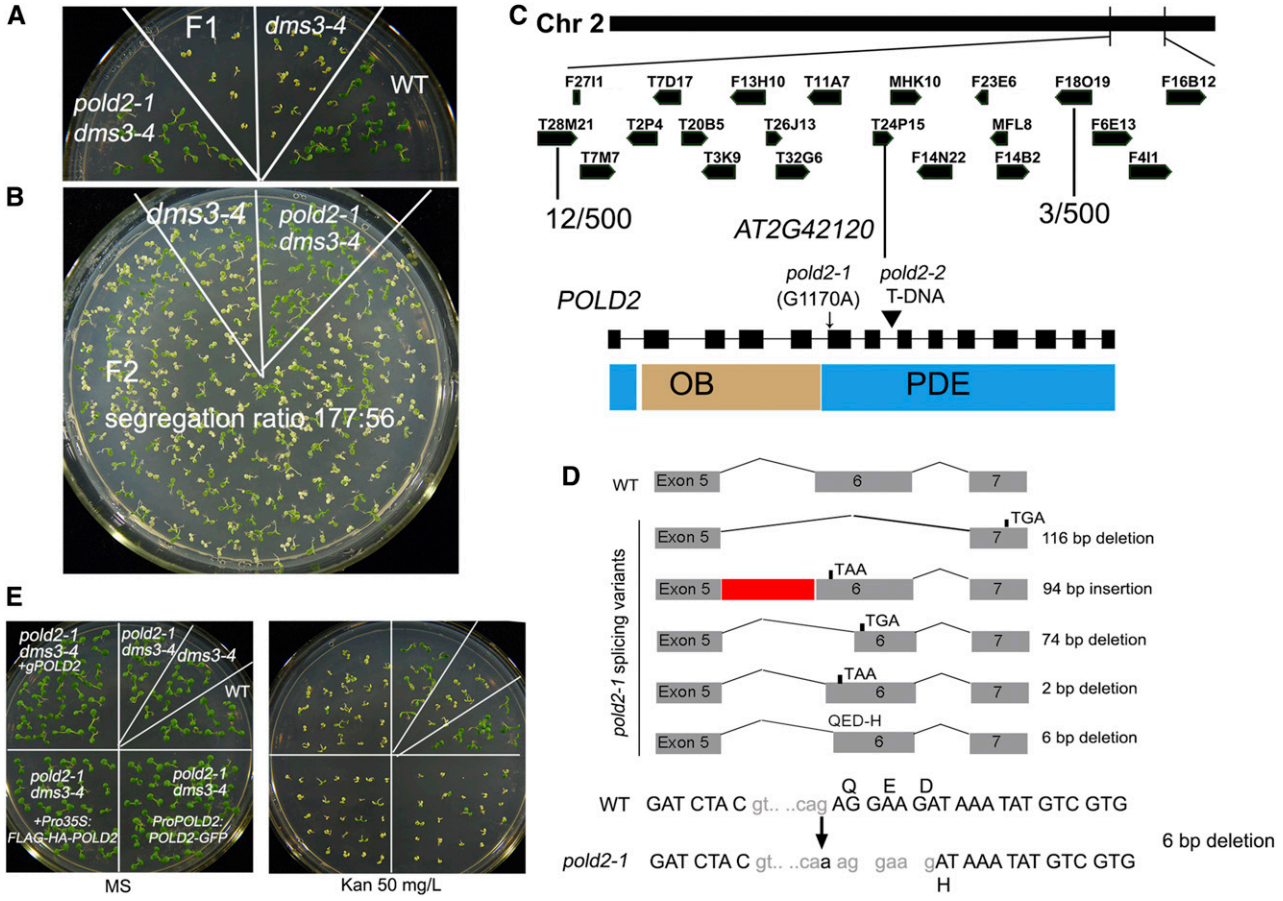

Figure 2. Map-based cloning of *POLD2*. A, Phenotypic analysis of F1 seedlings of *dms3-4 pold2-1* backcrossed with *dms3-4* on kanamycin-containing medium. B, The segregation of F2 seedlings growing on kanamycin-containing medium. C, Map-based cloning of the *pold2-1* mutation. The position of the *POLD2* mutation was narrowed to the bottom of chromosome 2 between BAC T28M21 and F18O19. The mutation of *pold2-1* occurred at splicing sites (G1170A). *pold2-2* is a T-DNA insertion allele. The domain structure of the POLD2 protein is indicated. OB, oligonucleotide-/oligosaccharide-binding domain; PDE, phosphodiesterase-like domain. D, Spliced forms of cDNA caused by the *pold2-1* mutation. Five kinds of transcripts were identified from 23 independent clones amplified from cDNAs. Among them, four transcripts would produce an earlier stop codon, and one would delete 6 bp and lead to the deletion of two amino acids (delete QE) and to the mutation of one amino acid (from original D to H). E, Complementary analyses of *pold2-1* with genomic DNA or *Pro35S:FLAG-HA-POLD2* construct, or native promoter driving cDNA (*ProPOLD2:POLD2-GFP*). Phenotypes of mutant and complementary lines growing on MS medium containing 0 mg/L kanamycin (left) or 50 mg/L kanamycin (right).

into heterozygous *pold2-2-/+* plants. Like the *pold2-1* mutant, the transgenic plants carrying *Pro35S:pold2-1* with homozygous T-DNA insertion were small (Supplemental Fig. S2C). These results suggest that this transcript from *pold2-1* is partially functional in plants. *ProPOLD2:GUS* expression indicated that *POLD2* is highly expressed in the shoot meristem, cotyledons, and older true leaves (Supplemental Fig. S3A). POLD2-GFP localization in transgenic plants indicated that POLD2 is a nuclear protein (Supplemental Fig. S3B).

Genetic Analysis of *POLD2* with Other DNA-Replication Proteins

To better characterize the genetic interactions between *POLD2* and other DNA-replication proteins, we crossed *pold2-1* with some DNA replication-related mutants and analyzed the phenotypes of the double mutants (Fig. 3). *pold2-1* mutant plants were much smaller and flowered earlier than the wild type (Fig. 3A). *pold2-1 polα* double mutants were smaller and exhibited more severe growth phenotypes than *polα* or *pold2-1* single mutants (Fig. 3A), suggesting that the two genes have additive effects on plant growth and development. In contrast, *polε polα* double mutants exhibited phenotypes similar to *polα* mutants (Fig. 3B), suggesting that *Polα* and *Polε* do not have additive effects on plant growth and work in the same pathway. The phenotypes of the *pold2-1 ror1-2* (*rpa2a*) and *polε ror1-2* double mutant were very similar to those of the *ror1-2* single mutant (Fig. 3, C and D), suggesting that *RPA2A* is a limiting factor for leading- and lagging-strand DNA replication. The *pold2-1 polε* double mutant was similar to

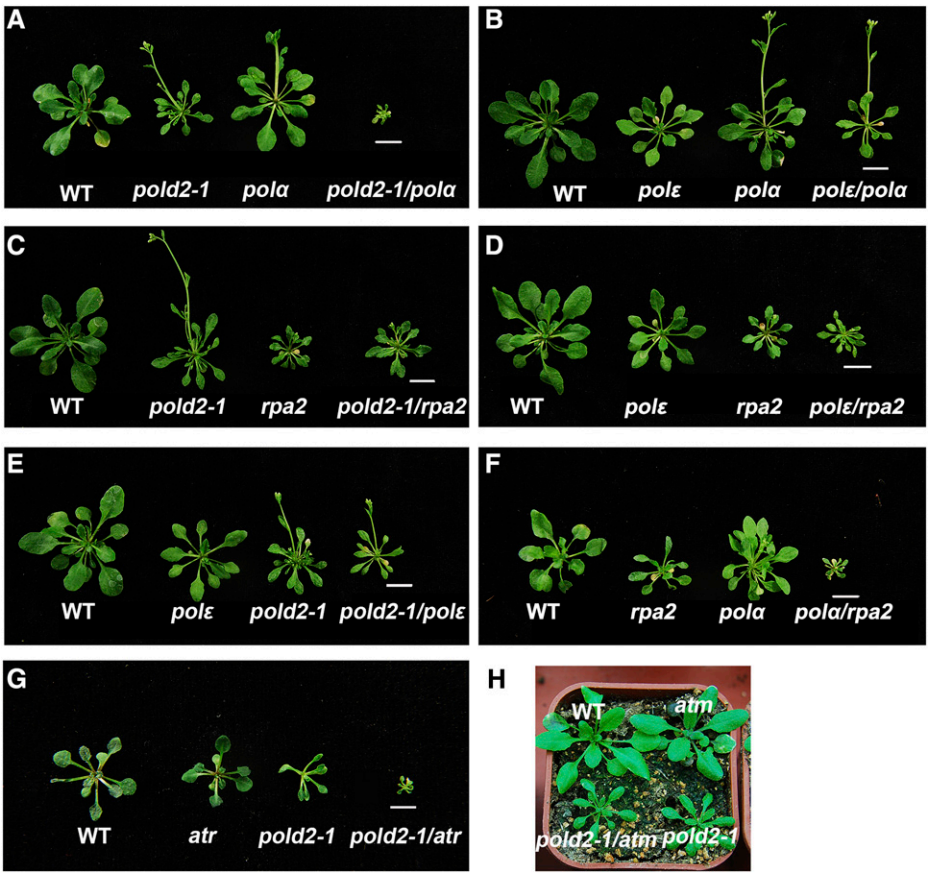

Figure 3. Phenotypic analyses of *pold2-1* with other DNA replication-related mutants. A, Phenotype of the wild type (WT), *pold2-1*, *polα*, and *pold2-1 polα* double mutant. B, Phenotype of the wild type, *polε*, *polα*, and *polε polα* double mutant. C, Phenotype of the wild type, *pold2-1*, *ror1-2* (*rpa2a*), and *pold2-1 ror1-2* double mutant. D, Phenotype of the wild type, *polε*, *ror1-2* (*rpa2a*), and *polε ror1-2* double mutant. E, Phenotype of the wild type, *polε*, *pold2-1*, and *pold2-1 polε* double mutant. F, Phenotype of the wild type, *ror1-2* (*rpa2a*), *polα*, and *polα ror1-2* double mutant. G, Phenotype of the wild type, *atr*, *pold2-1*, and *atr pold2-1* double mutant. H, Phenotype of the wild type, *atm*, *pold2-1*, and *atm pold2-1* double mutant. Bar = 1 cM.

pold2-1 (Fig. 3E), indicating that POLD2 acts at or has an epistasis effect on *Polε* for controlling plant development. Furthermore, *polα ror1-2* double mutants exhibited more severe growth phenotypes than *polα* or *ror1-2* single mutants (Fig. 3F), suggesting that *Polα* and *RPA2A* interact genetically in controlling plant growth (Fig. 3F).

ATR (Ataxia Telangiectasia-mutated and Rad3-related) is a DNA damage-activated protein kinase that is involved in the progression of DNA replication forks, and ATM (Ataxia Telangiectasia-Mutated) is a double-strand break-activated protein kinase. The *atr* mutant did not show a clear growth phenotype, and the *atm* mutant had a partially sterile phenotype relative to the wild type under normal growing conditions (Garcia et al., 2003; Culligan et al., 2004). The *pold2-1 atr* double mutant showed severe defects in leaf development and fertility (Fig. 3G), and the *pold2 atm* double mutant showed growth phenotypes similar to those of *pold2-1* (Fig. 3H). These results suggest that POLD2 and ATR have additive roles in controlling plant development.

The *pold2-1* Mutant Exhibits Sensitivity to DNA Damage, a Delayed Cell Cycle, Increased HR, and a Reduced Telomere Length

Previous studies indicated that DNA replication-related proteins have roles in controlling the cell cycle, HR, and genomic stability (Liu and Gong, 2011). In evaluating the effects of *POLD2* on these processes, we found that the *pold2-1* mutant was more sensitive to alkylating agent methyl methanesulfonate (MMS) than to the DNA-replication inhibitor hydroxyurea (HU) or to the DNA-interstrand crosslink-reagent cisplatin (Fig. 4, A and B). Quantitative real-time PCR (qRT-PCR) assessment of the expression of several genes that are responsible for DNA repair including *breast cancer susceptibility 1* (*BRCA1*), *RAD51*, *poly(ADP-ribose) polymerase 1* (*PARP1*), and *PARP2*. These genes were expressed at higher levels in *pold2-1* or *pold2-1 dms3-4* than in the wild type or *dms3-4* (Fig. 4C). To investigate cell cycle progression in the *pold2-1* mutant, we crossed *pold2-1* with the *ProCYCB1;1:GUS* reporter line (*CYCB1;1* is expressed during the G2/M transition and serves as a marker for cell cycle regulation). GUS activity in both the root and the shoot apical meristem was much stronger in *pold2-1* than in the wild type (Fig. 4D, a-d). RT-PCR confirmed that expression of the mitotic cyclin *CYCB1;1* was higher in *pold2*-1 than in the wild type (Fig. 4De). This result indicates that *pold2-1* delays the cell cycle.

We evaluated the frequency of HR in *pold2-1* by introducing the reporter line 651 (in C24 accession) into the *pold2-1*. Reporter line 651 carries an inverted orientation of the inactive GUS gene (Lucht et al., 2002).

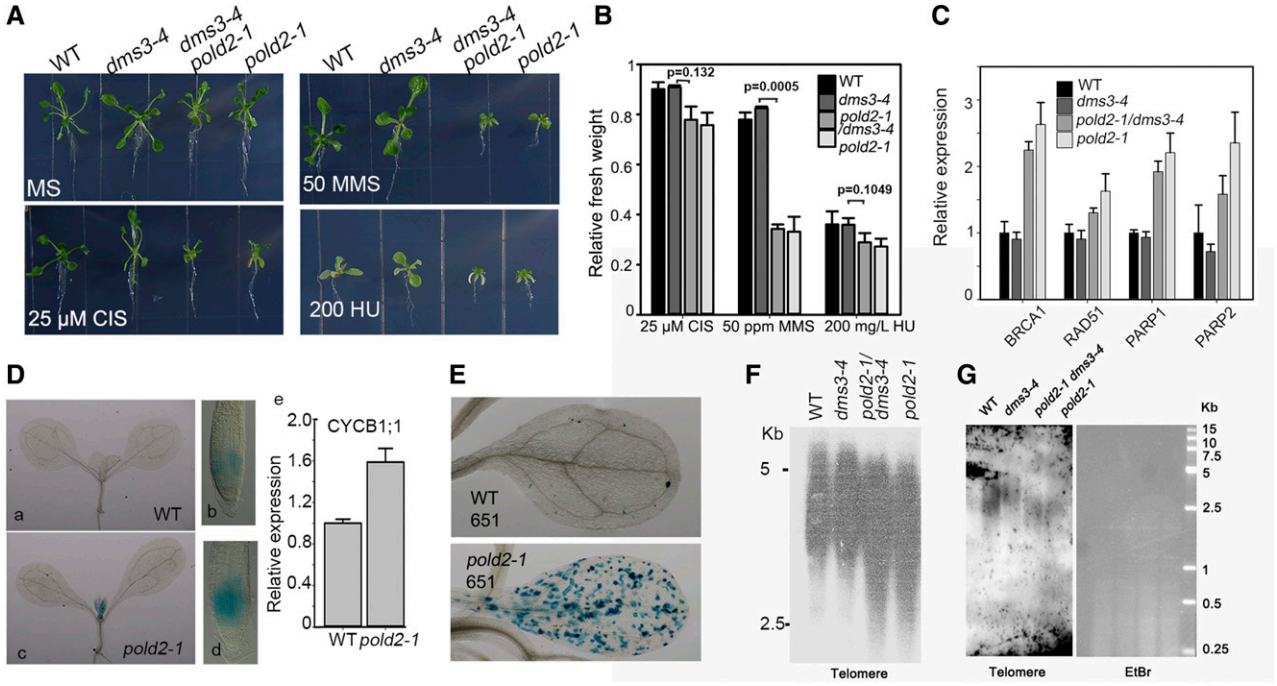

Figure 4. The *pold2-1* mutant has increased sensitivity to DNA damage, a delayed cell cycle, increased HR, and a reduced telomere length. A, *pold2-1* is hypersensitive to MMS. Wild-type (WT), *dms3-4*, *pold2-1 dms3-4*, and *pold2-1* seedlings that were grown for 15 d on MS medium alone or MS medium with 200 mg/L HU (200 HU), 50 ppm (65 μg mL^{-1}) MMS, or 25 μM cisplatin (25 CIS). *P*-values were calculated using Paired Student's *t* test. B, Relative fresh weight of seedlings in D. The fresh weight relative to untreated controls after treatment with DNA-damaging reagents is shown. Values are means ± SE, $n = 3$. C, Relative expression of DNA damage response genes in the wild type, *dms3-4*, *pold2-1 dms3-4*, and *pold2-1* as determined by qRT-PCR. RNAs extracted from 7-d-old seedlings were used for qRT-PCR. Values were normalized to the expression level of the references gene (*UBI*). Two independent experiments (each with three technical replicates) were done with similar results. Values are means ± SE, $n = 3$, from one experiment. D, *pold2-1* increases the expression of *ProCYCB1;1:GUS*. *ProCYCB1;1:GUS* was introduced into the *pold2-1* mutant by crossing the wild type carrying *ProCYCB1;1:GUS* with the *pold2-1* mutant. a to d, GUS staining in a wild-type seedling (a), a wild-type root tip (b), a *pold2-1* seedling (c), and a *pold2-1* root tip (d). e, *CYCB1;1* expression as determined by qRT-PCR. RNAs were extracted from 7-d-old seedlings and used for qRT-PCR. Values were normalized to the expression level of the references gene (*UBI*). Two independent experiments (each with three technical replicates) were done with similar results. Values are means ± SE, $n = 3$, from one experiment. E, *pold2-1* increases HR in 14-d-old seedlings. The wild-type 651 carrying a homologous reporter *GUS* gene was crossed with the *dms3-4 pold2-1* mutant. Homozygous *pold2-1* plants carrying the homozygous GUS reporter were isolated and used for GUS staining. F and G, *pold2-1* exhibits a reduced telomere length. Genomic DNAs of the wild type, *dms3-4*, *pold2-1*, and *pold2-1 dms3-4* digested by *Hin*fI (DNA-methylation sensitive, F) or *Mse*I (DNA-methylation insensitive, G) were subjected to Southern blot with a telomere probe.

A blue sector indicates that an intrachromosomal recombination event has reconstituted a functional GUS gene. As shown in Figure 4E, many more GUS staining sectors were observed in the cotyledons in *pold2-1* than in the wild type, suggesting that HR is negatively modulated by *POLD2*. A previous study indicated that mutations in the catalytic subunit of Pol δ (*POLD1*) result in genome instability and enhance the frequency of somatic intramolecular HR (Schuermann et al., 2009). We also found that the telomere was shorter in *pold2-1* or *pold2-1 dms3-4* than in the wild type or *dms3-4* (Fig. 4, F and G), suggesting that POLD2 is involved in modulating telomere length.

pold2-1-Released *NPTII* Silencing in *dms3-4* Is Independent of DNA Methylation

We used whole-genome BS-seq to determine whether DNA methylation is altered by *pold2-1*. Consistent with a previous study (Zhao et al., 2014), the *35S* promoter region had a high level of DNA methylation (Fig. 5A). The level of DNA methylation in *35S* was similar among *pold2-1*, *pold2-1 dms3-4*, *dms3-4*, and the wild type (Fig. 5B). Researchers have reported that, in *ros1* and some other related mutants, the DNA methylation level at the *NOS* region is increased (Zhao et al., 2014), which leads to the silencing of *NPTII*. Indeed, we found that DNA methylation and especially CG methylation is increased in the *dms3-4* mutant because of the reduced expression of *ROS1* (Li et al., 2012). The methylation level, however, is similar in *dms3-4* and *pold2-1 dms3-4* (Fig. 5C). Interestingly, the DNA methylation pattern in *pold2-1* is much more similar to that in the *pold2-1 dms3-4* or *dms3-4* mutant than to that in the wild type (Fig. 5C). This is probably because the *pold2-1* single mutant was obtained from the progeny of *pold2-1 dms3-4* crossed with the wild type, and the hyper DNA

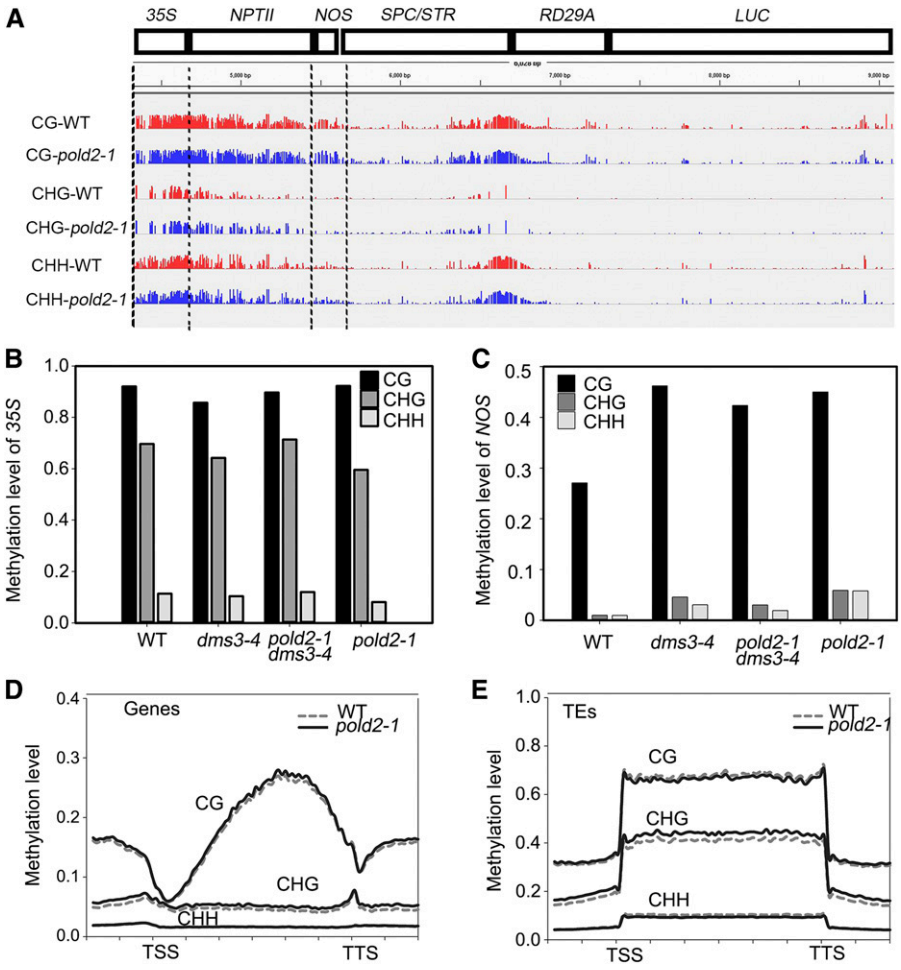

Figure 5. *pold2-1* releases the silencing of *NPTII* in *dms3-4* independent of DNA methylation. A, IGV visualization of the DNA methylation level (CG, CHG, and CHH) at the transgenic T-DNA locus in the wild type (WT) and *pold2-1* mutant from whole-genome bisulfite sequencing data. B and C, Methylation level of the *35S* (B) and *NOS* (C) regions of the wild type, *dms3-4*, *pold2-1*, and *dms3-4 pold2-1* as determined by bisulfite sequencing (10–15 clones were analyzed for each sample). D, Patterns of DNA methylation (CG, CHG, and CHH) across all genes in the wild type and the *pold2-1* mutant. Genes were aligned from the TSSs to the TTSs, and average methylation for all cytosines within each bin is plotted. E, Patterns of DNA methylation (CG, CHG, and CHH) across all transposon elements (TEs) in the wild type and the *pold2-1* mutant. Transposon elements were aligned from the TSSs to the TTSs, and average methylation for all cytosines within each bin is plotted.

methylation pattern was maintained after *dms3-4* was recovered. These results suggest that DNA methylation is not responsible for the release of the silencing of *NPTII* in the *dms3-4* mutant background.

We next checked DNA methylation on a genome-wide scale using the BS-seq. *pold2-1* mutant did not show a significantly altered DNA methylation level at the whole-genome scale (Fig. 5, D and E). In agreement with a previous study showing that the DNA single-stranded binding protein RPA2A does not affect DNA methylation (Elmayan et al., 2005; Stroud et al., 2013), POLD2 is dispensable for DNA methylation. These results suggest that the DNA replication machinery does not influence DNA methylation.

POLD2 Mediates H3K27me3 and H3K4me3 Histone Modification in *NPTII*

Given that POLD2 does not affect DNA methylation and that its mutation changes the expression of *NPTII*, we suspected that POLD2 may affect histone modification. We performed whole-genome ChIP-seq for H3K27me3, H3K4me3, H3K9me2, and H3 in the wild type and *pold2-1*.

Using ChIP-seq data, we compared the histone modification profiles on the T-DNA locus. The *35S* promoter region harbors a slightly higher level of H3K9me2 histone modification in *pold2-1* than in the wild type (Fig. 6, A and B). The *NPTII* region had decreased H3K27me3 and H3K4me3 but increased H3K9me2 in the *pold2-1* mutant compared to the wild type (Fig. 6, A and B). We next examined histone modification levels among the wild type, *dms3-4*, *pold-1 dms3-4*, and *pold2-1* using ChIP-PCR. We found that the H3K27me3 level at the *NPTII* gene body region was much lower in the *pold2-1* or *pold2-1 dms3-4* mutant than in the wild type or in the *dms3-4* mutant (Fig. 6D), which was consistent with the ChIP-seq data indicating that *pold2-1* decreased H3K27me3 (Fig. 6, A and B). The H3K9me2 level of both *35S* and *NPTII* was higher in *dms3-4* than in the wild type (Fig. 6, C and D), which would lead to a repression of *NPTII* gene expression in *dms3-4*. The H3K9me2 level in the *pold2-1 dms3-4* double mutant and in the *pold2-1* single mutant, however, was similar to that in the *dms3-4* mutant (Fig. 6, C and D), suggesting that the release of *NPTII* silencing in the *pold2-1* mutant in the *dms3-4* background was not due to changes in the H3K9me2 level. The H3K4me3 level

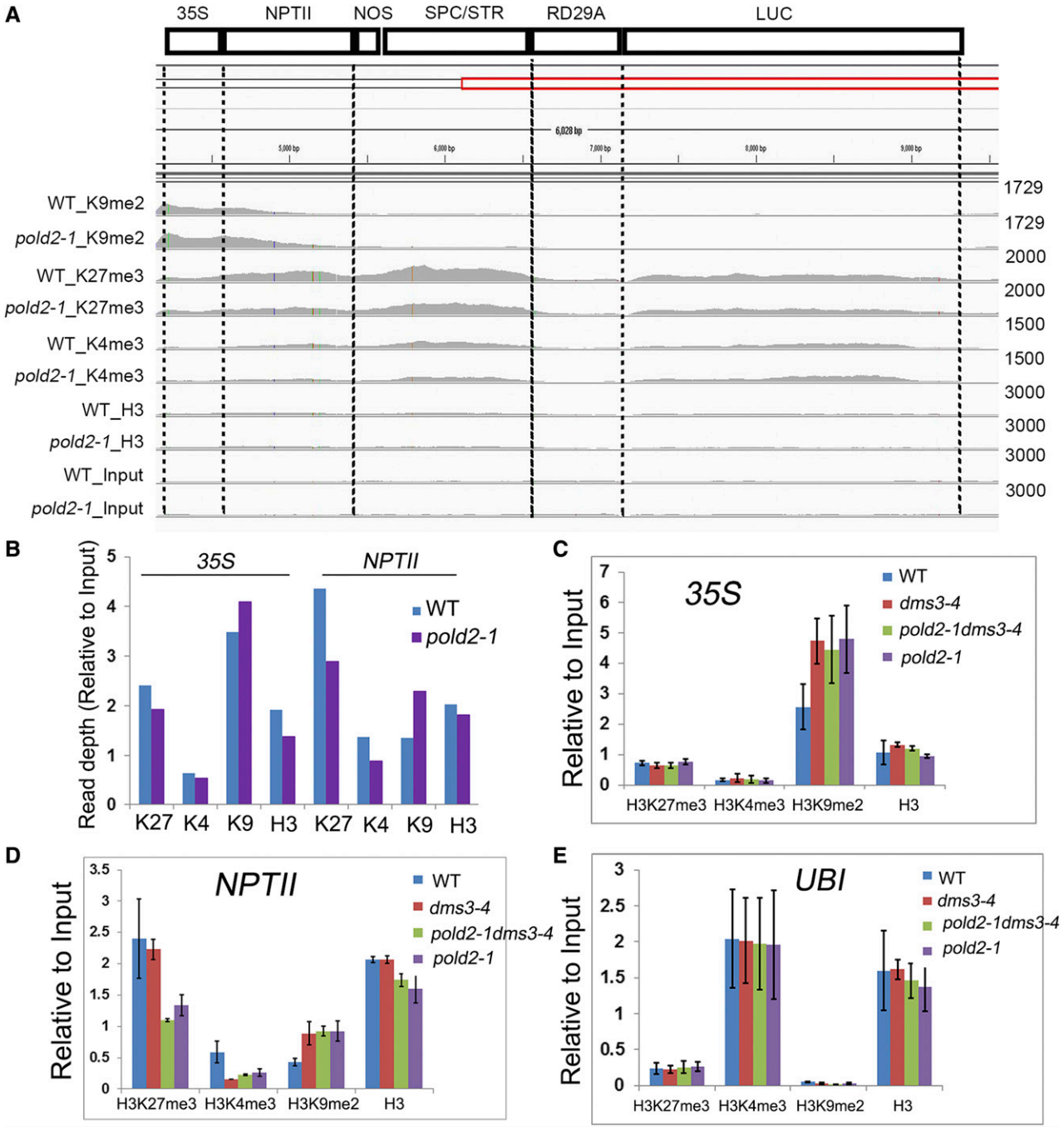

Figure 6. *pold2-1* decreases the H3K27me3 level at *NPTII*. A, Histone modification status of the transgene construct in the wild type (WT) and *pold2-1* mutant. Data of Histone H3 Lys 9 dimethylation (K9me2), Histone H3 Lys 27 trimethylation (K27me3), Histone H3 Lys 4 trimethylation (K4me3), total histone H3 (H3), and input (Input) level were shown from whole genome ChIP-seq. The data range of each modification was set to the same scale between the wild type and *pold2-1* mutant. B, Chart depicted the relative quantitative histone modification level of *35S* or *NPTII* region as shown in A. C-E, Histone modification levels at *35S* (C), *NPTII* (D), and *UBI* (E) in the wild type, *dms3-4*, *pold2-1 dms3-4*, and *pold2-1* as indicated by ChIP-PCR analysis. The histone modification levels of H3K27me3, H3K4me3, H3K9me2, and total histone H3 on each indicated locus were detected by ChIP-qPCR. *UBI* was used as a control locus enriched in H3K4me3 but depleted in H3K27me3 or H3K9me2 modification. The error bars represent the SEM.

in the *NPTII* region was lower in *dms3-4* than in the wild type (Fig. 6D). *pold2-1* mildly increased the H3K4me3 level in the *dms3-4* background, but the H3K4me3 level was still lower in the *pold2-1* background than in the wild type, which is consistent with the lower expression of *NPTII* in the *pold2-1* mutant (Figs. 1B and 6D).

Ubiquitin-conjugating enzyme 21 (*UBI*) was used as a positive control for H3K4me3 and as a negative control for H3K27me3 and H3K9me2, and the histone modification pattern on the *UBI* region was similar among the four samples (Fig. 6E). Together, these results suggest that the release of *NPTII* silencing in the *dms3-4* mutant by *pold2-1* results from a reduced level of H3K27me3.

We next sought to determine whether H3K27me3 or H3K4me3 is altered in the other mutants isolated from the same screen. Indeed, we found the H3K27me3 level on the *NPTII* was decreased in the *rfc1-4*, *ubp26-5*, and *hda6-11* mutants compared to that in the wild type (Supplemental Fig. S4A). We also found that *rfc1-4* and *ubp26-5* could partially restore the level of H3K4me3 in the *dms3-4* background (Supplemental Fig. S4B). *hda6-11* greatly increased H3K4me3, and the expression level of *NPTII* was higher in the *hda6-11* mutant than other mutants (Supplemental Fig. S4B; Figure 1B). These results suggest that *RFC1*, *UBP26*, and *HDA6* are also involved in mediating H3K27me3 and H3K4me3 modification and *NPTII* expression.

Correlation between Changes in Levels of H3K27me3 or H3K4me3 and Changes in Gene Expression in the *pold2-1* Mutant

We identified 7,786 genes with H3K27me3 (Supplemental Fig. S5A; Supplemental Table S1), and these genes largely overlap with those identified in two previous studies: they overlap with 85.4% (4,346 of 5,090; Supplemental Fig. S5A) of the genes previously identified in a ChIP-seq study (Lu et al., 2011) and with 83.4% (4,154 of 4,980; Supplemental Fig. S5A) of those genes previously identified in another ChIP-chip analysis (Zhang et al., 2007). We identified 17,849 genes with H3K4me3, and these genes overlap with 97.8% (13,899 of 14,206; Supplemental Table S2) of those reported by Luo et al. (2012; Supplemental Fig. S5A). H3K9me2 is mainly localized on TEs (Supplemental Fig. S5B). We also found 3,697 genes that harbor H3K9me2 (Supplemental Table S3), and these genes overlap with 73% (836 of 1,147) of those reported by Luo et al. (2012; Supplemental Fig. S5A). Overall, these results indicate that our ChIP-seq data are reliable.

Based on ChIP-seq data, we found 977 genes whose H3K27me3 levels were lower in the *pold2-1* mutant than in the wild type [*P*-value < 0.01, false discovery rate (FDR) < 0.01; Supplemental Table S4]. After plotting the epigenetic profile of these 977 genes with decreased levels of H3K27me3, we found that the H3K27me3 level was lower on the gene body in the *pold2-1* mutant than in the wild type (Fig. 7A). The H3K4me3 levels in these 977 genes were relatively low. The H3K4me3 signal is mainly detected after the transcriptional start site (TSS), the level of which was higher in *pold2-1* than in the wild type (Fig. 7A). The total H3 was enriched on these gene body regions but depleted on the TSS or transcription termination sites (TTS; Fig. 7A), which was consistent with a previous report (Ha et al., 2011). The level of total H3 was slightly lower in the *pold2-1* mutant than in the wild type (Fig. 7A). To determine whether changes in H3K27me3 were correlated with changes in gene expression, we performed RNA-seq of the wild type and the *pold2-1* mutant (Supplemental Table S5). Among the 977 genes with reduced levels of H3K27me3 in *pold2-1*, 385 were found to be expressed, of which, 282 genes (73%) were up-regulated. After plotting these 385 expressed genes using a heat map and a box plot, we found that the expression levels of these genes were significantly higher in *pold2-1* than in the wild type (*P*-value < 0.0001, paired Student's *t* test; Fig. 7, B and C). These results suggest that *pold2-1* leads to a decrease in H3K27me3 level, which in turn may increase gene expression.

We found 343 genes that had a significantly higher level of H3K27me3 in the *pold2-1* mutant than in the wild type (*P*-value < 0.01, FDR < 0.01; Supplemental Table S6). The increased H3K27me3 modification mainly occurred on the gene body regions (Fig. 7D). Among these genes, there were no obvious changes in H3K4me3 or in H3 between *pold2-1* and the wild type (Fig. 7D). Of the 343 genes with increased levels of H3K27me3, 117 were expressed (71 down-regulated and 46 up-regulated), but the expression was not significantly different between *pold2-1* and the wild type (Fig. 7, E and F; *P*-value = 0.2292, paired Student's *t* test). These results suggest that the moderate increase in H3K27me3 level in *pold2-1* does not apparently change the gene expression.

We found 499 genes that had significantly higher H3K4me3 levels in the *pold2-1* mutant than in the wild type (*P*-value < 0.01, FDR < 0.01; Supplemental Table S7), and 21.4% (107 of 499) of these genes overlapped with genes with decreased levels of H3K27me3. After plotting the epigenetic profiles of these 499 genes, we found that the increased H3K4me3 signals began to occur just after the TSS (the first nucleosome in the gene body) and then spread to the whole gene body and that their level was lowest at the TTS (Fig. 8A). The H3 level was slightly lower in the *pold2-1* mutant than in the wild type (Fig. 8A). Most of these 499 genes were expressed (455 of 499), and more than 76% (345 of 455) genes were up-regulated. After statistical analysis, the expression levels were significantly higher in the *pold2-1* mutant than in the wild type (Fig. 8, B and C; *P*-value < 0.0001, paired Student's *t* test). Only 32 of the genes were found to have a lower H3K4me3 level (*P*-value < 0.01, FDR < 0.01; Supplemental Table S8; Fig. 8D). Among these 32 genes, 30 were found to be expressed, of which 23 showed a lower expression level in the *pold2-1* mutant compared to the wild type. After boxplotting of these 30 genes, they exhibited a lower expression level (Fig. 8, E and F; *P*-value = 0.0023, paired Student's *t* test) in *pold2-1* than in the wild type. These results suggest that the *pold2-1* mutation prominently increases the H3K4me3 level and gene expression.

We further selected some loci for validation by ChIP-PCR. *SEP3* was recently reported to be a target of the

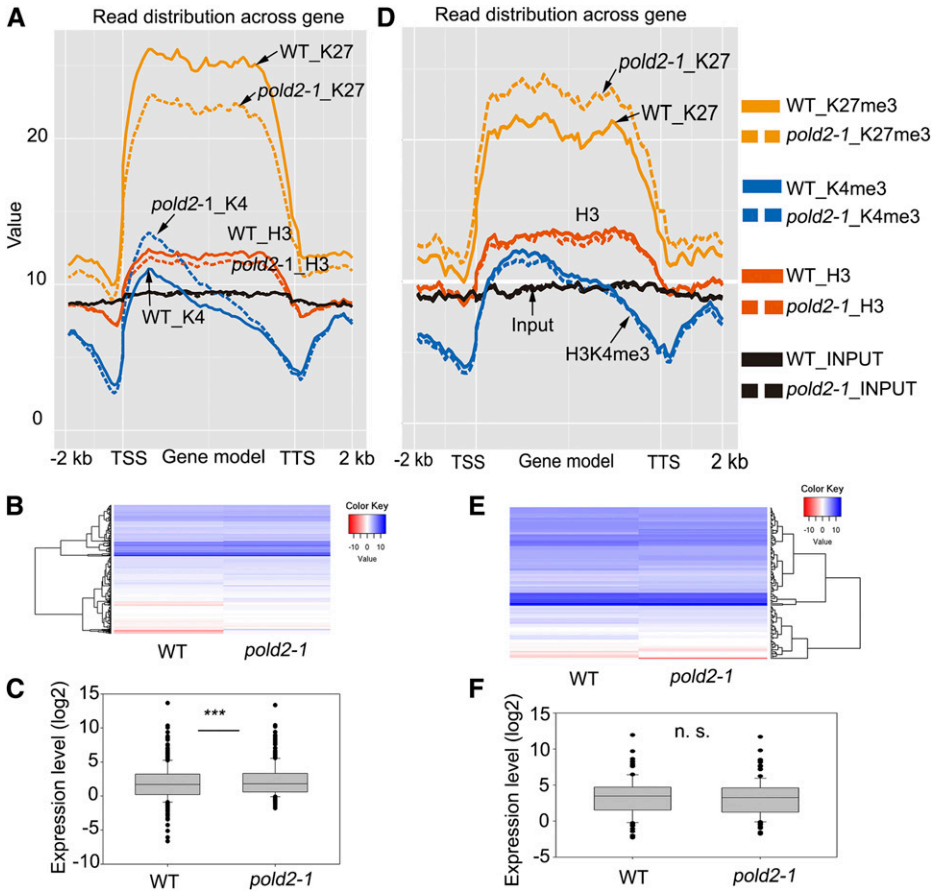

Figure 7. Correlation between H3K27me3 signals across the genes and mRNA expression levels caused by the *pold2-1* mutation. A, Altered histone modification profiles of 977 H3K27me3-decreased genes by *pold2-1*. Genes were aligned from the TSSs to the TSSs and divided into 60 bins. The 2,000-bp (2-kb) regions either upstream of TSS or downstream TTS were also included and divided into 20 bins, respectively. Histone modification levels of each bin are plotted. B, Gene expression profiles of H3K27me3-decreased genes in *pold2-1* and the wild type. Values were log2FPKM-transformed. FPKM were generated from RNA-seq using TopHat and Cufflinks software. C, Boxplot showing the expression (log2FPKM-transformed) of genes in B. The mean value of the group was significantly higher in *pold2-1* than in the wild type (*** $P < 0.0001$, two-tailed paired Student's *t* test). D, Altered histone modification profiles of 343 H3K27me3-increased genes by *pold2-1* mutant. Genes were aligned from the TSSs to the TTSs and divided into 60 bins. The 2,000-bp (2-kb) regions either upstream of TSS or downstream TTS were also included, and each was divided into 20 bins. Histone modification levels of each bin are plotted. E, Gene expression profiles of H3K27me3-increased genes in *pold2-1*. Values shown are log2FPKM-transformed. FPKM (fragments per kilobase of transcript per million mapped reads) were generated from RNA-seq using TopHat and Cufflinks software. F, Boxplot showing the expression (log2FPKM-transformed) of genes in B. The mean value of the group in *pold2-1* was not significantly different from that in the wild-type group (n.s., not significant, paired Student's *t* test).

catalytic subunit *POLD1*, and its H3K4me3 level is increased in the *pold1* mutant (Iglesias et al., 2015). Consistent with our ChIP data (Fig. 9A), *SEP3* together with eight other selected genes had decreased H3K27me3 levels and increased H3K4me3 levels. Two genes (*AT2G39250* and *AT1G06360*) with increased H3K27me3 and decreased H3K4me3 in *pold2 -1* relative to the wild type were also checked by ChIP-PCR (Fig. 9, B and C). The levels of total histone H3 among these genes were similar between the *pold2-1* mutant and the wild type (Fig. 9D). *UBI*, which has only a slight modification in H3K27me3 but a substantial modification in H3K4me3, and H3 were used as controls. Consistently, six of nine genes that had decreased H3K27me3 levels but increased H3K4me3 levels had higher expression levels in *pold2-1* than in the wild type (Fig. 9E). In contrast, the expression levels of *AT2G39250* and *AT1G06360* (with an increased level of H3K27me3 and a decreased level of H3K4me3) were lower in *pold2-1* than in the wild type (Fig. 9E). Together, these results suggest a critical role of *POLD2* in mediating H3K27me3 and H3K4me3 levels and gene expression.

DISCUSSION

Genetic screens for the release of the TGS of *Pro35S:NPTII* in either the *ros1* or *dms3-4* mutant has identified most

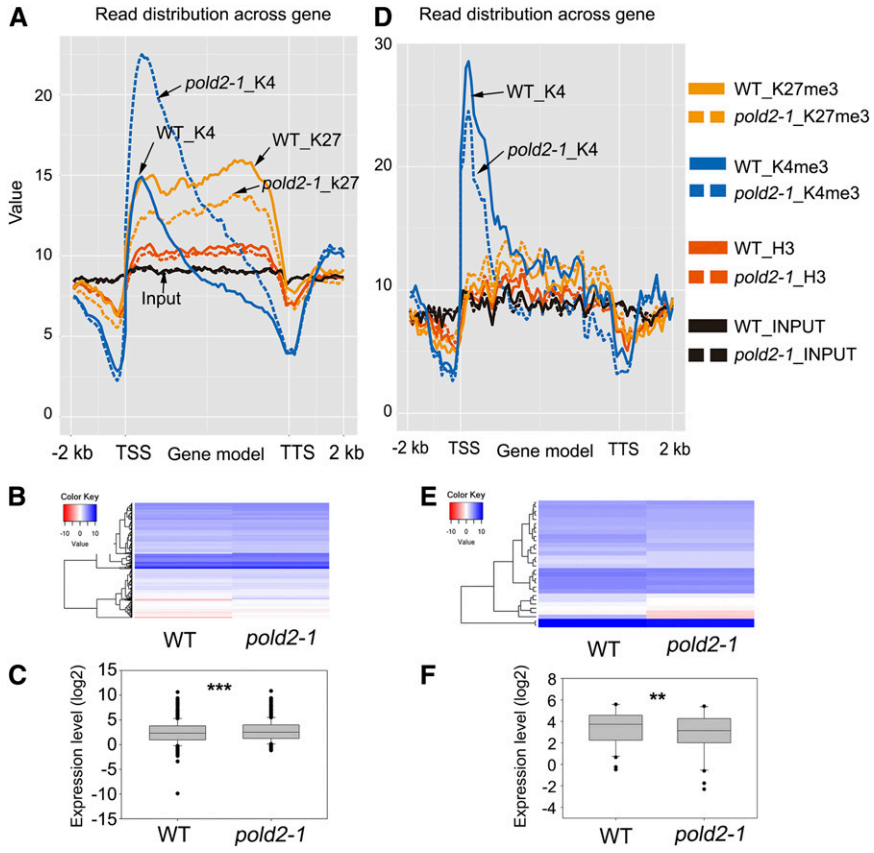

Figure 8. Correlation between H3K4me3 signals across the gene and mRNA expression levels caused by *pold2* mutant. A, Altered histone modification profiles of 499 H3K4me3-increased genes by *pold2-1*. Genes were aligned from the TSSs to the TTSs and divided into 60 bins. The 2,000-bp (2-kb) regions either upstream of TSS or downstream TTS were also included, and each was divided into 20 bins. Histone modification levels of each bin are plotted. B, Gene expression profiles of H3K4me3-increased genes by *pold2-1*. Values shown are log2FPKM. FPKM (fragments per kilobase of transcript per million mapped reads) was generated from RNA-seq using TopHat and Cufflinks software. C, Boxplot showing the expression (log2FPKM-transformed) of genes in B. The mean value of the *pold2-1* group was significantly higher than that of the wild-type group (*** $P < 0.0001$, two-tailed, paired Student's *t* test). D, Altered histone modification profiles of 32 H3K4me3-decreased genes by *pold2-1* mutant. Genes were aligned from the TSSs to the TTSs and divided into 60 bins. The 2,000-bp (2-kb) regions either upstream of TSS or downstream TTS were also included, and each was divided into 20 bins. Histone modification levels of each bin are plotted. E, Gene expression profiles of H3K4me3-decreased genes by *pold2-1* mutant. Values are log2FPKM-transformed. FPKM was generated from RNA-seq using TopHat and Cufflinks software. F, Boxplot showing the expression (log2FPKM) of genes in B. The mean value of the *pold2-1* group was significantly lower than that of the wild-type group (** $P < 0.001$, two-tailed paired Student's *t* test).

of the core DNA-replication proteins, including the DNA single-strand-binding protein RPA2A (Xia et al., 2006), Polα (Liu et al., 2010a), Pol ε (Yin et al., 2009), POLD2 (this study), RFC1 (Liu et al., 2010b), and TOUSLED protein kinase (Wang et al., 2007). Other studies have identified other DNA replication-related proteins involved in mediating TGS, including BRU1 (Takeda et al., 2004), chromatin assembly factor (CAF-1) subunits FAS1 and FAS2 (Ono et al., 2006; Schonrock et al., 2006), and TEBICHI (Inagaki et al., 2009). The release of TGS by defects in the DNA-replication machinery suggests that these processes must have a common mechanism. In this study, we found that *POLD2* does not affect DNA methylation but plays crucial roles in regulating H3K27me3 and H3K4me3 modification according to genome-wide ChIP-seq. The released silencing of *NPTII* in *dms3-4* is mainly due to the change in histone modifications by *pold2-1*. These results suggest that the DRR-TGS pathway is essential for maintaining H3K27me3 and H3K4me3 inheritance and gene expression.

DNA Pol δ is conserved in eukaryotes and is important in regulating genomic stability and development in Arabidopsis (Schuermann et al., 2009; Iglesias et al., 2015). To our knowledge, the biological functions of *Arabidopsis POLD2* have not been studied yet. In this study, we found that *POLD2* is an essential gene that contributes to DNA replication, genomic stability through maintaining HR, DNA damage repair, and telomere length. In addition, genetic analysis presents a

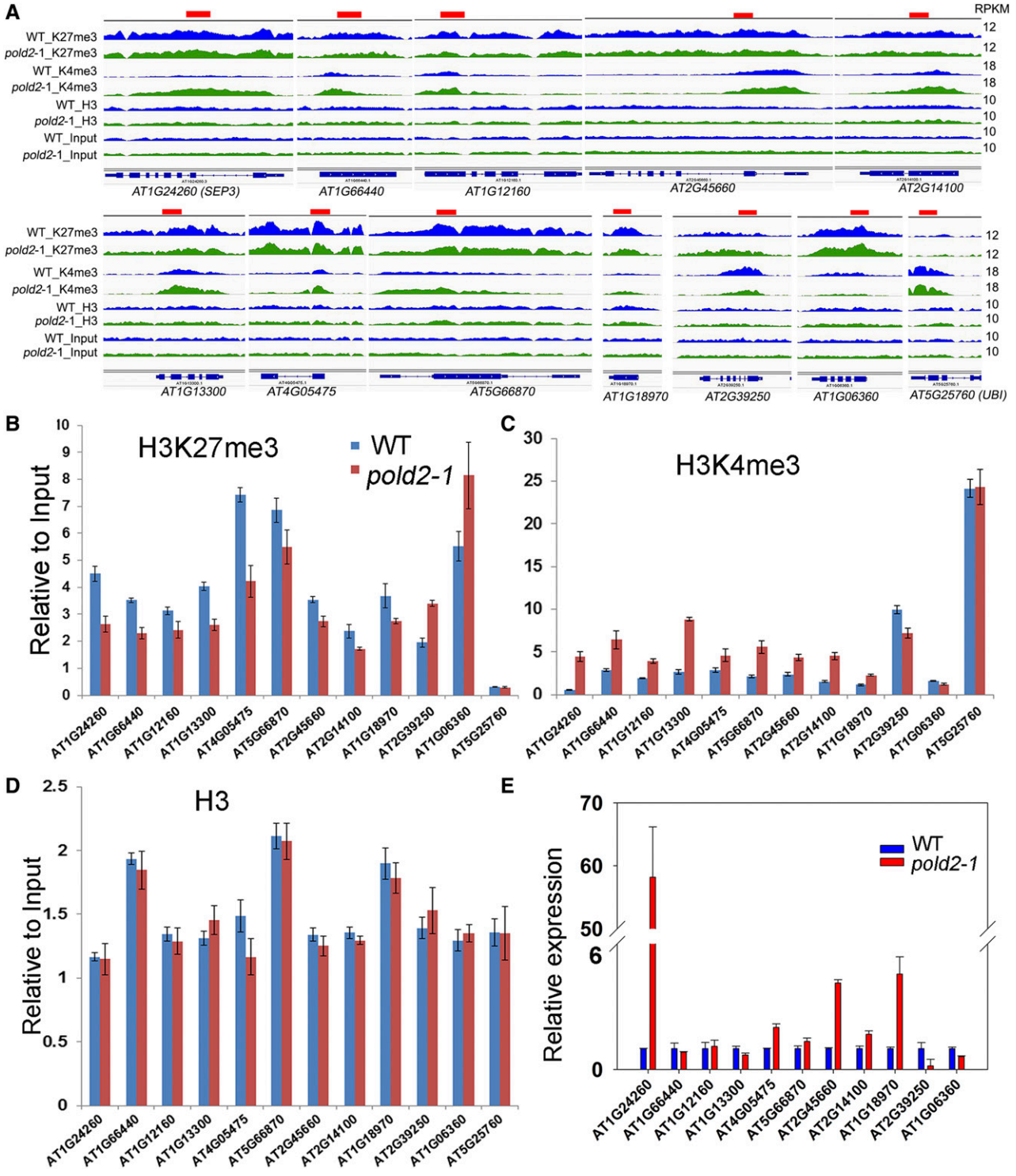

Figure 9. IGV visualization of selected histone modification altered genes, and validation of ChIP-seq results. A, IGV views of reads density (RPKM) of H3K27me3 (K27me3), H3K4me3 (K4me3), H3, and Input from ChIP-seq data in the wild type (WT) and *pold2-1* mutant. The data range of each modification was set to the same scale for the wild type and *pold2-1* mutant. *AT2G39250* and *AT1G06360* are examples of genes with increased levels of H3K27me3 and decreased levels of H3K4me3. *UBI* is a positive control for H3K4me3 and a negative control for H3K27me3; the level of histone modification for *UBI* was similar for the wild type and the *pold2-1* mutant. The other genes had decreased levels of H3K27me3 and increased levels of H3K4me3. The red bars on the top of each gene indicate the primer location used for validation. B to D, ChIP-qPCR verified the selected histone modification changed genes. The histone modification level of H3K27me3 (B), H3K4me3 (C), and total histone H3 (D) on each indicated gene

synergistic role of *POLD2* with *ATR* or *Polα* in controlling plant development (Fig. 3). Similarly, a previous study reported that TEBICHI protein containing both DNA helicase and polymerase domains genetically interacts with ATR to regulate plant development (Inagaki et al., 2009).

DNA replication proteins play crucial roles in maintaining histone inheritance. RNA- and ChIP-seq indicate that POLD2 mediates the expression of genes enriched in H3K27me3 and H3K4me3 in gene bodies. We found a high correlation between reduced H3K27me3 levels or increased H3K4me3 levels and increased gene expression, which is consistent with previous studies in Arabidopsis (Zhang et al., 2009) and *Drosophila* (Papp and Muller, 2006). However, the expression of genes with increased H3K27me3 levels in *pold2-1* does not show a clear tendency toward reduced gene expression, probably because their expression is already very low or because the experimental seedlings have mixed cell types; the obtained results might be over- or underestimated. In this case, we might not detect the difference if change occurs in only a small proportion of the cells in the whole plant. Perhaps future studies on specific cell types or cell cycles will be able to prove how DNA replication factors participate in epigenetic regulation in Arabidopsis. Interestingly, in embryonic stem cells, a specific chromatin-modification pattern (chromatin areas with these patterns are termed bivalent domains and harbor both H3K27me3 and H3K4me3) is important for cell differentiation and memory (Bernstein et al., 2006). Our results indicate that the *POLD2* mutation altered the levels of H3K27me3 and H3K4me3 of 107 bivalent genes (Supplemental Fig. S6; Supplemental Table S9). These results suggest that POLD2 is involved in regulating the bivalent histone modifications and that the DNA replication machinery could contribute to cell differentiation and cell-type transition.

So far, the intrinsic mechanism that DNA replication affected H3K27me3 or H3K4me3 was not clear, although several lines of evidence suggest that DNA replication or related factors help regulate PcG target genes. Our RNA-seq data indicate that the *POLD2* mutation did not change the expression of genes responsible for the establishment and maintenance of H3K4me3 and H3K27me3 significantly (Supplemental Table S10). Western-blot analyses indicate that the total levels of H3K4me3 and H3K27me3 were not changed in *pold2* mutant (Supplemental Fig. S7). These results suggest that POLD2 does not affect the expression of genes for establishment and maintenance of H3K4me3 and H3K27me3 modification, or the global H3K4me3 and H3K27me3 levels. It was previously proposed that DNA polymerase δ may play a role in preventing replication stress or HR and in depositing active H3K4me3 marks (Iglesias et al., 2015). Meanwhile, some studies indicate that the catalytic subunit of DNA polymerase α interacts with (Barrero et al., 2007) or perturbs the binding of like-heterochromatin protein 1 (LHP1; Hyun et al., 2013), which is the main reader/effector for H3K27me3 in Arabidopsis (Barrero et al., 2007; Zhang et al., 2007). Another link between DNA replication and H3K27me3 is MSI1 (multicopy suppressor of ira1), a chromatin assembly factor in Arabidopsis, which interacts with PcG protein and LHP1 (Derkacheva et al., 2013). So, it is possible that a dysfunctional Pol δ may disturb the entire replication machinery, which would interfere with the recruitment of LHP1 or PcG proteins to PcG targets. In mammalian cells, PcG proteins can be phosphorylated by cyclin-dependent kinases in a cell cycle-dependent manner (Chen et al., 2010). Because *pold2-1* exhibits an abnormal cell cycle (Fig. 4D), it is also possible that a disordered cell cycle machinery in the DNA replication-related mutants may influence the activity of PcG proteins and subsequently epigenetic silencing. Further studies will be needed to dissect the molecular mechanisms for how each component of the DNA replication machinery participates in this process.

MATERIALS AND METHODS

Plant Materials and Growth Conditions

pold2-1, *hda6-11*, *ubp26-5*, and *rfc1-4* were isolated from an EMS-mutagenized population of *dms3-4* in this study. *ros1* (*ros1-1*), *polε* (*abo4*), *polα*, *rpa2a-2* (*ror1-2*), *dms3-4*, *nrpd1-8*, *nrpe1-14*, and *ros4* are C24 ecotypes carrying homozygous *ProRD29A:LUC* and *Pro35S:NPTII* transgenes. *GK-762B02* (*pold2-2*; Rosso et al., 2003), *atr-2* (SALK_032841C), and *atm* (SALK_040423C) are T-DNA insertion mutants ordered from ABRC. *dms3-1* (Col-0; Kanno et al., 2008) is a gift from Dr. Matzke.

Seeds were sterilized and grown on MS medium plates supplemented with 20 g/L Suc and 0.8% agar at 22°C under long-day (23 h) illumination. Then 7-d-old seedlings were transferred to soil and grown in a greenhouse at 22°C under long-day (16 h) conditions.

Map-Based Cloning of *POLD2*

Approximately 12,000 *dms3-4* (C24 background and kanamycin-sensitive) seeds were mutated with EMS. The putative mutants were isolated from M2 seedlings that survived on MS medium containing 50 mg/L kanamycin. For map-based cloning of the *POLD2* gene, *pold2-1 dms3-4* (in C24) was crossed with *dms3-1* (Col-0; Kanno et al., 2008), and 250 kanamycin-resistant plants selected from the F2 progeny were analyzed with SSLP markers based on the polymorphism data (http://1001genomes.org/). *POLD2* was narrowed to an area between BAC clone F18O19 and T28M21. Based on previous results with DNA polymerases, the *POLD2* gene was selected and sequenced and a point mutation was determined.

Figure 9. (*Continued.*)
was measured by ChIP-qPCR between the wild type and *pold2-1* mutant. Values presented are relative to the input, the error bars represent the SEM ($n = 3$). *AT5G25760* (*UBI*) was used as a control locus enriched in H3K4me3 modification but depleted in H3K27me3 modification. E, Relative gene expression level of these selected genes. RNAs extracted from 10-d-old seedlings were used for qRT-PCR. Values were normalized to the expression level of the references gene (*UBI*). Two independent experiments (each with three technical replicates) were done with similar results. Values are means ± SE, $n = 3$, from one experiment.

For complementation, a 4.9-kb length of *POLD2* genomic DNA containing 1,932 bp (promoter + 5′UTR) and 254 bp 3′UTR was cloned into pCAMBIA1391. The plasmid was introduced into *pold2-1 dms3-4* mutants by *Agrobacterium tumefaciens* strain GV3101.

Subcellular Localization of POLD2-GFP Fusion Protein

Three fragments, that is, the 1,932-bp promoters of *POLD2*, *POLD2* cDNA without the TAA stop codon, and *GFP* cDNA, were obtained using paired primers and were separately cloned into the pCAMBIA1300 vector with *POLD2* fused in frame with *GFP*. The vector was introduced into *pold2-1 dms3-4* plants by *A. tumefaciens* strain GV3101. This construct was able to complement the *pold2-1* mutant, indicating that the POLD2-GFP fusion protein was functional. Three-day-old seedlings of the T2 progeny were examined and photographed with a confocal laser scanning microscope (Leica sp5).

GUS Staining

A 1,932-bp genomic fragment of *POLD2* upstream of ATG was amplified and cloned into the pCAMBIA1391 vector. This *ProPOLD2:GUS* plasmid was then transformed into the wild type (C24 ecotype) by *A. tumefaciens* strain GV3101. At least 25 independent transgenic lines were selected for GUS staining. Transgenic plants at different growth stages were collected and stained with freshly made GUS staining buffer (1× phosphate-buffered saline, 0.1% Triton X-100, 0.5 mM $K_3Fe(CN)_6$, 1 mg/mL X-Gluc) at 37°C, and were then washed several times with 70% ethanol.

Histochemical Assay of *ProCYCB1;1:GUS*

Arabidopsis (*Arabidopsis thaliana*) plants transformed with *ProCYCB1;1:GUS* (Colon-Carmona et al., 1999) were crossed with the *pold2-1* mutant. Three independent lines homozygous for both GUS reporter and *pold2-1* were selected from F4 progeny and subjected to histochemical GUS staining. Homozygous GUS reporter wild-type lines selected from F4 progeny were used as the control.

Intrachromosomal HR Assay

The intrachromosomal recombination reporter line 651 (Molinier et al., 2006; in C24) was crossed with the *pold2-1dms3-4* double mutant. At least three independent F4 plants homozygous for the mutant *pold2-1* (*DMS3/DMS3*×*pold2-1/pold2-1*) or wild type (*DMS3/DMS3*×*POLD2/POLD2*) and homozygous for the GUS transgene were selected. Seedlings were subjected to histochemical GUS staining as mentioned above.

BS-Seq

A whole-genome BS-seq library was prepared mainly according to Urich et al. (2015). Genomic DNAs were extracted from seedlings using the DNeasy Plant Mini Kit (QIAGEN) according to the manufacturer's instructions. A 2-μg quantity of genomic DNAs was sonicated (20 cycles of 30 s on, 30 s off, at low intensity) into 200-bp fragments with a Bioruptor (Diagenode), end repaired, 3′-dA-tailed, and ligated to methylated adapters. After purification, the ligated DNA fragments were treated with the EZ Methylation-Gold Kit (Zymo Research). The eluted bisulfite-treated DNAs were amplified using barcoded primers for sequencing (CGCTGT for the wild type and ACAGTG for the *pold2* mutant). High-throughput sequencing of the BS-seq library was performed on the Illumina NextSEquation 500 System with single-end 75-bp reads. The raw sequence data were demultiplexed and converted to fastq files using bcl2fastq2 Conversion Software (version v2.16.0) under default parameters. The DNA methylation was analyzed according to Zhao et al. (2014) and Wang et al. (2015).

For locus-specific bisulfite sequencing, 500-ng of DNA was treated with the EZ Methylation-Gold Kit (Zymo Research). Two eluted fractions (10 μL each) were used as PCR templates for amplifying the target sequence; the primers were the same as previously reported (Zhao et al., 2014). Products were cloned into the pMD18-T vector (TaKaRa), and 10 to 15 independent clones of each sample were sequenced (Lifetech-China).

Analysis of RNA-Seq Data

Total RNAs extracted from seedlings using the RNeasy Plant Mini Kit (QIAGEN) were used for sequencing on the Illumina platform. Three biological replicates were performed for *pold2-1* and the wild type. Paired-end reads were selected and aligned to the Arabidopsis reference genome (version: TAIR10) (Lamesch et al., 2012) using TopHat and Cuffdiff (Trapnell et al., 2012). Values of each sample used for heatmap and boxplot were log2 (FPKM)-transformed. Fragments per kilobase of transcript per million mapped reads (FPKM) was generated from the output of the Cuffdiff software.

ChIP Assay

ChIP assay was based on the previous studies (Zhang et al., 2007; Lu et al., 2011) with some modifications. A 2-g quantity of 10-d-old seedlings was fixed in 1% formaldehyde. The seedlings were ground into power with liquid nitrogen and homogenized with nuclei extraction buffer (1 M hexylene glycol, 20 mM Tris-HCl, pH 8.0, 0.15 mM spermine, 5 mM 2-mercaptoethanol, 1% Triton X-100, 0.1 mM phenylmethylsulfonyl fluoride, and protease inhibitor cocktail). The homogenates were filtered through Miracloth and centrifuged at 2,000 *g* for 10 min at 4°C. The pellets were washed two times with nuclei extraction buffer and resuspended in 300 μL of nuclei lysis buffer (50 mM Tris-HCl, pH 8.0, 10 mM EDTA, 1% SDS, and protease inhibitor cocktail). The chromatin was sonicated (15 cycles of 30 s on with 30 s off, at high intensity) into fragments of about 300 bp using a Bioruptor. The antibodies used were anti-H3K27me3 (Ab6002, Abcam), anti-H3 (ab1791, Abcam), anti-H3K4me3 (ab8580, Abcam), and anti-H3K9me2 (ab1220, Abcam). Dynabeads (10001D, Life Technologies) were used for immunoprecipitation. After RNase A and Proteinase K treatment, DNAs were recovered using the QIAquick PCR purification kit (QIAGEN). The DNA concentration was determined using the Qubit 2.0 system (Life Technologies). The ChIP and input samples were adjusted with dH_2O to a concentration of 50 pg/μL and used for qRT-PCR. Real-time PCR was performed in 20 μL with 1 μL of immunoprecipitated or input DNA in SYBR Green Master Mix (TaKaRa). The reaction conditions were as follows: 95°C for 5 min and 40 cycles of 95°C for 30 s and 60°C for 1 min.

A 10-ng quantity of ChIP or input DNA was used to prepare a high-throughput sequencing library. End repair, dA-tailing, adapter ligation, and amplification were carried out using the NEBNext ChIP-Seq Library Prep Master Mix Set for Illumina (E6240, NEB) according to the manufacturer's protocol. Index primers used for each sample were as follows: ATCACG for WT-H3K27me3, CGATGT for WT-H3K4me3, TTAGGC for WT-H3K9me2, TGACCA for WT-H3, ACAGTG for WT-Input, GCCAAT for pold2-H3K27me3, CAGATC for pold2-H3K4me3, ACTTGA for pold2-H3K9me2, GATCAG for *pold2*-H3, and TAGCTT for *pold2*-Input. High-throughput sequencing of the ChIP-seq library was carried on the Illumina NextSEquation 500 System with single-end 75-bp reads. The raw sequence data were demultiplexed and converted to fastq files using bcl2fastq2 Conversion Software (version v2.16.0) under default parameters.

ChIP-Seq Analysis

Reads were mapped to the Arabidopsis genome (TAIR10) using bowtie1 (version 0.12.9; Langmead et al., 2009) allowing two nucleotide mismatches using the following parameters: bowtie -q -k 1 -n 2 -l 36–best -S -p 2. Mapped reads were de-duplicated and sorted by samtools (version 0.1.19-44428cd; Li et al., 2009). Then the reads were normalized to read depth and used for further analysis. Peaks were found using MACS software (version 1.4.2; Zhang et al., 2008) using H3 as a background. For H3K27me3 peaks finding in the wild type as an example, the parameters were as follows: macs14 -t WT_K27ME3.sorted.bam –c WT_H3.sorted.bam –f BAM -g 1.30e+8 -n WT_K27ME3–shiftsize 73–pvalue 1e-5–bw = 300–mfold = 10,30. Gene annotation was used BEDTools (Quinlan and Hall, 2010) according to TAIR10.

Histone modification changes between the wild type and *pold2-1* mutant were determined with SICER software (version 1.1; Zang et al., 2009). For H3K4me3, the parameters were as follows: SICER-df.sh pold2-1-H3K4me3.bed pold2-1-input.bed WT-H3K4me3.bed WT-input.bed 200 200 0.05 0.05; this means that the Window size and Gap size were set at 200 bp. Then filtered by P-value < 0.01, FDR < 0.01, and fold change > 1.5. For H3K27me3, the parameters were as follows: SICER-df.sh pold2-1-H3K27me3.bed pold2-1-input.bed WT-H3K27me3.bed WT-input.bed 200 200 0.05 0.05, then filtered by P-value < 0.01, FDR < 0.01. Different regions were annotated with BEDTools. Figures 7 and 8 were made using R packages (ggplot2, Rmisc, and reshape) and homemade script.

Real-Time PCR

Total RNAs were extracted from 0.1 g of seedlings using the RNeasy Plant Mini Kit (QIAGEN). After RNase-free DNaseI(TaKaRa) digestion at 37°C, 4 μg of RNA was reverse transcribed with Moloney murine leukemia virus reverse transcriptase (Promega) in a 30-μL volume. A 2-μL volume of 5-fold-diluted cDNA was added to a 20-μL real-time PCR reaction system in SYBR Green Master Mix (TaKaRa). The reaction was running by StepOnePlus Real-Time PCR System (Applied Biosystems), and the procedure was as follows: 95°C for 2 min followed by 40 cycles of 95°C for 5 s and 60°C for 30 s. Specific primers for each gene are listed in Supplemental Table S11. *UBIQUITIN-CONJUGATING ENZYME 21* (*UBI*, *AT5G25760*) was used as the reference gene as previously described (Huettel et al., 2006). Three technical replicates were performed per biological replicate, and two to three biological replicates were used in all experiments.

DNA-Damage Assay

A DNA-damage assay was performed as previously described (Liu et al., 2010b). Seeds were sterilized and grown on MS medium or MS medium supplemented with one of three DNA-damaging reagents: 25 μM cis-diamineplatinum (II) dichloride (SIGMA, 479306), 50 ppm (0.005%, 65 μg mL^{-1}) MMS (SIGMA, 129925), or 200 mg/L HU (SIGMA, H8627). After they were grown for 15 d at 22°C under long-day (23 h) illumination, seedlings were imaged and weighed. The fresh weight relative to untreated controls after treatment with DNA-damaging reagents was calculated. Three biological replicates were carried out.

Telomere Length

Genomic DNAs were extracted from 14-d-old seedlings using the DNaesy Plant Mini Kit (QIAGEN) according to the manufacturer's instructions. A 3-μg quantity of DNA was digested with *Hin*fI or *Mse*I in a 100-μL system at 37°C. Southern blot was performed with the DIG-High Prime DNA Labeling and Detection Starter Kit II (Roche). The synthesized telomere repeat (TTTAGGG), which was labeled with digoxigenin using the DIG Oligonucleotide 3′-End Labeling Kit (Roche), was used as the probe.

Accession Numbers

Sequence data from this article can be found in the EMBL/GenBank data libraries under accession numbers: POLD2 (AT2G42120), RFC1 (AT5G22010), POLA (AT5G67100), POLE (AT1G08260), ROR1 (AT2G24490), ROS1(AT2G36490), DMS3 (AT3G49250), NRPD1 (AT1G63020), NRPE1 (AT2G40030), ROS4 (AT3G14980), ATM (AT3G48190), ATR (AT5G40820), HDA6 (AT5G63110), UBP26 (AT3G49600),, SEP3 (AT1G24260), UBI (AT5G25760), BRCA1 (AT4G21070), RAD51 (AT5G20850), PARP1 (AT2G31320), PARP2 (AT4G02390), and CYCB1;1 (AT4G37490).

RNA-seq, BS-seq, and ChIP-seq data have been deposited in the National Center for Biotechnology Information Gene Expression Omnibus (GEO) database under accession number GSE79259.

Supplemental Data

The following supplemental materials are available.

Supplemental Figure S1. Diagrams of hda*6-11*, *ubp26-5*, *rfc1-4*, and *pold2-1* mutations.

Supplemental Figure S2. Genetic analysis of *pold2-1* with *pold2-2*.

Supplemental Figure S3. *POLD2* is a nuclear protein and is ubiquitously expressed.

Supplemental Figure S4. ChIP-qPCR in *rfc1-4*, *ubp26-5*, and *hda6-11* samples.

Supplemental Figure S5. Validation of ChIP-seq data.

Supplemental Figure S6. Epigenetic profile of bivalent genes affected by *pold2-1* mutant.

Supplemental Figure S7. Western blot to check global H3K27me3 and H3K4me3 in the *pold2-1* mutant.

Supplemental Table S1. List of genes that harbor H3K27me3 in the C24 ecotype.

Supplemental Table S2. List of genes that harbor H3K4me3 in the C24 ecotype.

Supplemental Table S3. List of genes that harbor H3K9me2 in the C24 ecotype.

Supplemental Table S4. List of genes with decreased levels of H3K27me3 in the *pold2-1* mutant.

Supplemental Table S5. RNA-seq data.

Supplemental Table S6. List of genes with increased levels of H3K27me3 in the *pold2-1* mutant.

Supplemental Table S7. List of genes with increased levels of H3K4me3 in the *pold2-1* mutant.

Supplemental Table S8. List of genes with decreased levels of H3K4me3 in the *pold2-1* mutant.

Supplemental Table S9. Bivalent genes changed in the *pold2-1* mutant.

Supplemental Table S10. The expression of genes responsible for H3K27me3 and H3K4me3 in the wild type and *pold2-1* mutant from RNA-seq data.

Supplemental Table S11. Primers used in this study.

ACKNOWLEDGMENTS

We thank Dr. Marjori A. Matzke for providing *dms3-1* mutant. We also thank Arabidopsis Biological Resource Center for T-DNA mutant.

Received December 29, 2015; accepted April 24, 2016; published April 25, 2016.

LITERATURE CITED

Aufsatz W, Mette MF, van der Winden J, Matzke M, Matzke AJ (2002) HDA6, a putative histone deacetylase needed to enhance DNA methylation induced by double-stranded RNA. EMBO J **21:** 6832–6841

Barrero JM, Gonzalez-Bayon R, del Pozo JC, Ponce MR, Micol JL (2007) INCURVATA2 encodes the catalytic subunit of DNA Polymerase alpha and interacts with genes involved in chromatin-mediated cellular memory in Arabidopsis thaliana. Plant Cell **19:** 2822–2838

Bernstein BE, Mikkelsen TS, Xie X, Kamal M, Huebert DJ, Cuff J, Fry B, Meissner A, Wernig M, Plath K, et al (2006) A bivalent chromatin structure marks key developmental genes in embryonic stem cells. Cell **125:** 315–326

Burgers PM (2009) Polymerase dynamics at the eukaryotic DNA replication fork. J Biol Chem **284:** 4041–4045

Chen S, Bohrer LR, Rai AN, Pan Y, Gan L, Zhou X, Bagchi A, Simon JA, Huang H (2010) Cyclin-dependent kinases regulate epigenetic gene silencing through phosphorylation of EZH2. Nat Cell Biol **12:** 1108–1114

Church DN, Briggs SE, Palles C, Domingo E, Kearsey SJ, Grimes JM, Gorman M, Martin L, Howarth KM, Hodgson SV, et al (2013) DNA polymerase epsilon and delta exonuclease domain mutations in endometrial cancer. Hum Mol Genet **22:** 2820–2828

Colon-Carmona A, You R, Haimovitch-Gal T, Doerner P (1999) Technical advance: spatio-temporal analysis of mitotic activity with a labile cyclin-GUS fusion protein. Plant J **20:** 503–508

Culligan K, Tissier A, Britt A (2004) ATR regulates a G2-phase cell-cycle checkpoint in Arabidopsis thaliana. Plant Cell **16:** 1091–1104

Derkacheva M, Steinbach Y, Wildhaber T, Mozgova I, Mahrez W, Nanni P, Bischof S, Gruissem W, Hennig L (2013) Arabidopsis MSI1 connects LHP1 to PRC2 complexes. EMBO J **32:** 2073–2085

Elmayan T, Proux F, Vaucheret H (2005) Arabidopsis RPA2: a genetic link among transcriptional gene silencing, DNA repair, and DNA replication. Curr Biol **15:** 1919–1925

Garcia V, Bruchet H, Camescasse D, Granier F, Bouchez D, Tissier A (2003) AtATM is essential for meiosis and the somatic response to DNA damage in plants. Plant Cell **15:** 119–132

Gong Z, Morales-Ruiz T, Ariza RR, Roldan-Arjona T, David L, Zhu JK (2002) ROS1, a repressor of transcriptional gene silencing in Arabidopsis, encodes a DNA glycosylase/lyase. Cell **111:** 803–814

Ha M, Ng DW, Li WH, Chen ZJ (2011) Coordinated histone modifications are associated with gene expression variation within and between species. Genome Res **21:** 590–598

Huettel B, Kanno T, Daxinger L, Aufsatz W, Matzke AJ, Matzke M (2006) Endogenous targets of RNA-directed DNA methylation and Pol IV in Arabidopsis. EMBO J **25:** 2828–2836

Hyun Y, Yun H, Park K, Ohr H, Lee O, Kim DH, Sung S, Choi Y (2013) The catalytic subunit of Arabidopsis DNA polymerase alpha ensures stable maintenance of histone modification. Development **140:** 156–166

Iglesias FM, Bruera NA, Dergan-Dylon S, Marino-Buslje C, Lorenzi H, Mateos JL, Turck F, Coupland G, Cerdan PD (2015) The Arabidopsis DNA polymerase delta has a role in the deposition of transcriptionally active epigenetic marks, development and flowering. PLoS Genet **11:** e1004975

Inagaki S, Nakamura K, Morikami A (2009) A link among DNA replication, recombination, and gene expression revealed by genetic and genomic analysis of TEBICHI gene of Arabidopsis thaliana. PLoS Genet **5:** e1000613

Johnson RE, Klassen R, Prakash L, Prakash S (2015) A Major Role of DNA Polymerase delta in Replication of Both the Leading and Lagging DNA Strands. Mol Cell **59:** 163–175

Johnson RE, Prakash L, Prakash S (2012) Pol31 and Pol32 subunits of yeast DNA polymerase delta are also essential subunits of DNA polymerase zeta. Proc Natl Acad Sci USA **109:** 12455–12460

Kanno T, Bucher E, Daxinger L, Huettel B, Bohmdorfer G, Gregor W, Kreil DP, Matzke M, Matzke AJ (2008) A structural-maintenance-of-chromosomes hinge domain-containing protein is required for RNA-directed DNA methylation. Nat Genet **40:** 670–675

Kapoor A, Agarwal M, Andreucci A, Zheng X, Gong Z, Hasegawa PM, Bressan RA, Zhu JK (2005) Mutations in a conserved replication protein suppress transcriptional gene silencing in a DNA-methylation-independent manner in Arabidopsis. Curr Biol **15:** 1912–1918

Lamesch P, Berardini TZ, Li D, Swarbreck D, Wilks C, Sasidharan R, Muller R, Dreher K, Alexander DL, Garcia-Hernandez M, et al (2012) The Arabidopsis Information Resource (TAIR): improved gene annotation and new tools. Nucleic Acids Res **40:** D1202–D1210

Langmead B, Trapnell C, Pop M, Salzberg SL (2009) Ultrafast and memory-efficient alignment of short DNA sequences to the human genome. Genome Biol **10:** R25

Law JA, Jacobsen SE (2010) Establishing, maintaining and modifying DNA methylation patterns in plants and animals. Nat Rev Genet **11:** 204–220

Li H, Handsaker B, Wysoker A, Fennell T, Ruan J, Homer N, Marth G, Abecasis G, Durbin R, Genome Project Data Processing S (2009) The Sequence Alignment/Map format and SAMtools. Bioinformatics **25:** 2078–2079

Li X, Qian W, Zhao Y, Wang C, Shen J, Zhu JK, Gong Z (2012) Antisilencing role of the RNA-directed DNA methylation pathway and a histone acetyltransferase in Arabidopsis. Proc Natl Acad Sci USA **109:** 11425–11430

Liu J, Ren X, Yin H, Wang Y, Xia R, Wang Y, Gong Z (2010a) Mutation in the catalytic subunit of DNA polymerase alpha influences transcriptional gene silencing and homologous recombination in Arabidopsis. Plant J **61:** 36–45

Liu Q, Gong Z (2011) The coupling of epigenome replication with DNA replication. Curr Opin Plant Biol **14:** 187–194

Liu Q, Wang J, Miki D, Xia R, Yu W, He J, Zheng Z, Zhu JK, Gong Z (2010b) DNA replication factor C1 mediates genomic stability and transcriptional gene silencing in Arabidopsis. Plant Cell **22:** 2336–2352

Lu F, Cui X, Zhang S, Jenuwein T, Cao X (2011) Arabidopsis REF6 is a histone H3 lysine 27 demethylase. Nat Genet **43:** 715–719

Lucht JM, Mauch-Mani B, Steiner HY, Metraux JP, Ryals J, Hohn B (2002) Pathogen stress increases somatic recombination frequency in Arabidopsis. Nat Genet **30:** 311–314

Luo C, Sidote DJ, Zhang Y, Kerstetter RA, Michael TP, Lam E (2013) Integrative analysis of chromatin states in Arabidopsis identified potential regulatory mechanisms for natural antisense transcript production. Plant J **73:** 77–90

Miyabe I, Mizuno K, Keszthelyi A, Daigaku Y, Skouteri M, Mohebi S, Kunkel TA, Murray JM, Carr AM (2015) Polymerase delta replicates both strands after homologous recombination-dependent fork restart. Nat Struct Mol Biol **22:** 932–938

Molinier J, Ries G, Zipfel C, Hohn B (2006) Transgeneration memory of stress in plants. Nature **442:** 1046–1049

Murfett J, Wang XJ, Hagen G, Guilfoyle TJ (2001) Identification of Arabidopsis histone deacetylase HDA6 mutants that affect transgene expression. Plant Cell **13:** 1047–1061

Ono T, Kaya H, Takeda S, Abe M, Ogawa Y, Kato M, Kakutani T, Mittelsten Scheid O, Araki T, Shibahara K (2006) Chromatin assembly factor 1 ensures the stable maintenance of silent chromatin states in Arabidopsis. Genes Cells **11:** 153–162

Palles C, Cazier JB, Howarth KM, Domingo E, Jones AM, Broderick P, Kemp Z, Spain SL, Guarino E, Salguero I, et al (2013) Germline mutations affecting the proofreading domains of POLE and POLD1 predispose to colorectal adenomas and carcinomas. Nat Genet **45:** 136–144

Papp B, Muller J (2006) Histone trimethylation and the maintenance of transcriptional ON and OFF states by trxG and PcG proteins. Genes Dev **20:** 2041–2054

Prindle MJ, Loeb LA (2012) DNA polymerase delta in DNA replication and genome maintenance. Environ Mol Mutagen **53:** 666–682

Probst AV, Dunleavy E, Almouzni G (2009) Epigenetic inheritance during the cell cycle. Nat Rev Mol Cell Biol **10:** 192–206

Probst AV, Fagard M, Proux F, Mourrain P, Boutet S, Earley K, Lawrence RJ, Pikaard CS, Murfett J, Furner I, et al (2004) Arabidopsis histone deacetylase HDA6 is required for maintenance of transcriptional gene silencing and determines nuclear organization of rDNA repeats. Plant Cell **16:** 1021–1034

Quinlan AR, Hall IM (2010) BEDTools: a flexible suite of utilities for comparing genomic features. Bioinformatics **26:** 841–842

Ramirez-Parra E, Gutierrez C (2007) E2F regulates FASCIATA1, a chromatin assembly gene whose loss switches on the endocycle and activates gene expression by changing the epigenetic status. Plant Physiol **144:** 105–120

Rosso MG, Li Y, Strizhov N, Reiss B, Dekker K, Weisshaar B (2003) An Arabidopsis thaliana T-DNA mutagenized population (GABI-Kat) for flanking sequence tag-based reverse genetics. Plant Mol Biol **53:** 247–259

Schonrock N, Exner V, Probst A, Gruissem W, Hennig L (2006) Functional genomic analysis of CAF-1 mutants in Arabidopsis thaliana. J Biol Chem **281:** 9560–9568

Schuermann D, Fritsch O, Lucht JM, Hohn B (2009) Replication stress leads to genome instabilities in Arabidopsis DNA polymerase delta mutants. Plant Cell **21:** 2700–2714

Sridhar VV, Kapoor A, Zhang K, Zhu J, Zhou T, Hasegawa PM, Bressan RA, Zhu JK (2007) Control of DNA methylation and heterochromatic silencing by histone H2B deubiquitination. Nature **447:** 735–738

Steimer A, Amedeo P, Afsar K, Fransz P, Mittelsten Scheid O, Paszkowski J (2000) Endogenous targets of transcriptional gene silencing in Arabidopsis. Plant Cell **12:** 1165–1178

Stroud H, Greenberg MV, Feng S, Bernatavichute YV, Jacobsen SE (2013) Comprehensive analysis of silencing mutants reveals complex regulation of the Arabidopsis methylome. Cell **152:** 352–364

Takeda S, Tadele Z, Hofmann I, Probst AV, Angelis KJ, Kaya H, Araki T, Mengiste T, Mittelsten Scheid O, Shibahara K, et al (2004) BRU1, a novel link between responses to DNA damage and epigenetic gene silencing in Arabidopsis. Genes Dev **18:** 782–793

Trapnell C, Roberts A, Goff L, Pertea G, Kim D, Kelley DR, Pimentel H, Salzberg SL, Rinn JL, Pachter L (2012) Differential gene and transcript expression analysis of RNA-seq experiments with TopHat and Cufflinks. Nat Protoc **7:** 562–578

Urich MA, Nery JR, Lister R, Schmitz RJ, Ecker JR (2015) MethylC-seq library preparation for base-resolution whole-genome bisulfite sequencing. Nat Protoc **10:** 475–483

Wang C, Dong X, Jin D, Zhao Y, Xie S, Li X, He X, Lang Z, Lai J, Zhu JK, et al (2015) Methyl-CpG-binding domain protein MBD7 is required for active DNA demethylation in Arabidopsis. Plant Physiol **167:** 905–914

Wang Y, Liu J, Xia R, Wang J, Shen J, Cao R, Hong X, Zhu JK, Gong Z (2007) The protein kinase TOUSLED is required for maintenance of transcriptional gene silencing in Arabidopsis. EMBO Rep **8:** 77–83

Xia R, Wang J, Liu C, Wang Y, Wang Y, Zhai J, Liu J, Hong X, Cao X, Zhu JK, et al (2006) ROR1/RPA2A, a putative replication protein A2, functions in epigenetic gene silencing and in regulation of meristem development in Arabidopsis. Plant Cell **18:** 85–103

Yin H, Zhang X, Liu J, Wang Y, He J, Yang T, Hong X, Yang Q, Gong Z (2009) Epigenetic regulation, somatic homologous recombination, and abscisic acid signaling are influenced by DNA polymerase epsilon mutation in Arabidopsis. Plant Cell **21:** 386–402

Zang CZ, Schones DE, Zeng C, Cui KR, Zhao KJ, Peng WQ (2009) A clustering approach for identification of enriched domains from histone modification ChIP-Seq data. Bioinformatics **25:** 1952–1958

Zhang X, Bernatavichute YV, Cokus S, Pellegrini M, Jacobsen SE (2009) Genome-wide analysis of mono-, di- and trimethylation of histone H3 lysine 4 in Arabidopsis thaliana. Genome Biol **10:** R62

Zhang X, Clarenz O, Cokus S, Bernatavichute YV, Pellegrini M, Goodrich J, Jacobsen SE (2007) Whole-genome analysis of histone H3 lysine 27 trimethylation in Arabidopsis. PLoS Biol **5:** e129

Zhang Y, Liu T, Meyer CA, Eeckhoute J, Johnson DS, Bernstein BE, Nussbaum C, Myers RM, Brown M, Li W, et al (2008) Model-based Analysis of ChIP-Seq (MACS). Genome Biol **9:** R137

Zhao Y, Xie S, Li X, Wang C, Chen Z, Lai J, Gong Z (2014) REPRESSOR OF SILENCING5 Encodes a Member of the Small Heat Shock Protein Family and Is Required for DNA Demethylation in Arabidopsis. Plant Cell **26:** 2660–2675

Zhu JK (2009) Active DNA demethylation mediated by DNA glycosylases. Annu Rev Genet **43:** 143–166